CALIFORNIA INSTITUTE OF TECHNOLOGY

DYNAMIC PROPERTIES LABORATORY

Some High Temperature Oxidation Characteristics Of Nickel With Chromium Additions

by
Gordon Everett Zima

83

A REPORT ON RESEARCH CONDUCTED UNDER
CONTRACT WITH THE OFFICE OF NAVAL RESEARCH

April 1956

SOME HIGH TEMPERATURE OXIDATION CHARACTERISTICS OF NICKEL WITH CHROMIUM ADDITIONS

by

Gordon Everett Zima

Seventh Technical Report

under
Office of Naval Research
Contract N6onr-24430
Project Designation NR 031-355

California Institute of Technology
Pasadena, California

April 1956

ACKNOWLEDGEMENTS

The author wishes to thank Professors Pol Duwez, F. S. Buffington and D. S. Clark for the suggestions and technical assistance which have made this work possible. He appreciates the interest and cooperation of Professor V. F. Schomaker. To Mr. R. Willens the author is indebted for the preparation of some of the alloys used in this study.

The author is grateful to the Naval Ordnance Test Station in Pasadena for substantial financial support over most of this work. For support of the later work, he wishes to thank the Office of Naval Research.

ABSTRACT

The relationship between alloy chromium content and oxidation rate has been determined for nickel-chromium alloys containing up to 17At°/o chromium. The tests were conducted at 1096C, under one atmosphere of oxygen. The observed structural and phase changes in the oxide were related to the oxidation rate. It has been found that increasing amounts of chromium in the NiO phase govern the oxidation rate for alloys containing less than 2At°/o chromium. For alloys of greater than 2At°/o chromium, a complex exchange of chromium among three phases--NiO, Cr_2O_3 and the spinel, $NiCr_2O_4$--has been detected. This chromium exchange was reflected in the lattice parameter of the NiO phase, and in the rate of increase of oxidation rate with chromium addition to the alloy. The present work indicates that an interstitial diffusion mechanism may become dominant in the oxides of high chromium content. Within the scope of the present work, the high oxidation stability of nickel-chromium alloys has been correlated with the presence of Cr_2O_3 in the oxide layer.

Oxidation rates for high purity nickel have been determined at temperatures of 980, 1096, and 1260C, under one atmosphere of oxygen. The present data, combined with lower temperature data obtained by Gulbransen and Andrew, yielded an activation energy of 45.1Kcal/mole for the oxidation of nickel.

TABLE OF CONTENTS

LIST OF FIGURES

LIST OF FIGURES (Cont'd)

LIST OF TABLES

I. INTRODUCTION

The description of the process of formation of a gas-metal reaction product has progressed from simple phenomenological statements, relating weight gain to exposure time, to the present theories which attempt to detail the gas-metal reaction at the molecular level. Most of the theory of the gas-metal reaction has developed without reference to a specific gas. Metal deterioration by the action of oxygen, bromine, fluorine, etc. has been encompassed by one theory and these specific reactions are of equal theoretical, if not practical, importance. The word oxidation is thus somewhat restrictive in discussing the process under consideration.

The bulk of the oxidation work has employed materials of commercial interest. In addition, much of the work has been conducted under actual, or simulated, industrial exposure conditions. Considering the multitude of variables operating in tests where the material and atmosphere compositions are complex and partially controlled, the remarkable inconsistencies which have characterized much published oxidation data are not surprising.

Present knowledge of the interactions of the components in a binary alloy during oxidation is extremely limited. The characteristics of the pure components cannot be superposed to gain a prediction of the alloy behavior. Semi-conductor studies of recent years have shown that great changes in electrical properties can be effected by minute additions of certain elements

to the parent substance. In many instances, the oxidation behavior also appears to be very sensitive to changes in the composition of the metal. A systematic study of binary alloys would seem to take precedence over attempts to analyze the oxidation behavior of the complex alloy systems presented by modern high temperature alloys. The securing of oxidation rate data for these latter materials is a relatively simple matter. However, the recommendations for improving the oxidation stability of these materials do not appear to have a satisfactory theoretical, or empirical, basis at the present time.

The present work is concerned with some effects of small chromium additions on the oxidation characteristics of high purity nickel. The nickel-chromium system has been the subject of extensive oxidation study principally because of the high oxidation resistance of certain nickel-chromium and nickel-chromium-iron alloys. Most of this work has involved material of high ($>20 At^{o}/o$) chromium content. Some studies of small chromium additions have shown that the effect of the first chromium additions is to increase the oxidation rate. This augmentation effect of chromium reportedly persists up to a chromium content near $10 At^{o}/o$. With further chromium addition, the familiar high oxidation stability of nickel-chromium alloys is rapidly attained. The present work attempts to define this reported maximum in the oxidation rate in somewhat greater detail and to relate the observed oxidation behavior to the physical and chemical structure of the oxide.

II. BACKGROUND DISCUSSION

The first quantitative statements concerning the gas-metal reaction are attributed to Tammann (1)* and Pilling and Bedworth (2). One of the products of this work on monometal oxidation was the parabolic growth law. Using the parameters weight gain per unit area (M) and exposure time (θ), the parabolic law may be expressed:

$$M^2 = K_p \theta \qquad (1)$$

where K_p is the parabolic rate constant, usually given in $gm^2 cm^{-4} sec^{-1}$. The parabolic law is obeyed by one type of diffusion controlled process. If it is assumed that the concentrations of the diffusant at the metal-oxide and oxide-gas interfaces are constant, then the concentration gradient will be inversely proportional to the oxide thickness. Assuming that the rate of increase of the oxide thickness is proportional to the concentration gradient, then Eq. 1 is obtained from integration of the rate equation, after expressing the oxide growth as weight gain per unit area. Considering the possibilities for departure from this simple picture, it is surprising that a number of metals, such as nickel, cadmium and zinc, obey the parabolic law in some oxidation environments.

The oxidation of some monometals and alloys obeys a linear type law. Employing the same parameters as above, the linear law may be expressed:

$$M = K_l \theta \qquad (2)$$

---

*Numbers in parentheses apply to references given at end of text.

The linear law could be expected when the oxidation process is controlled by an interface reaction. If this reaction is constant with time, the linear law is obtained upon integration of the rate expression. The linear law is observed for metals generating porous, or volatile oxides. The continual exposure of the metal surface fulfills the requirement for an interface controlled oxidation. Barium exposed to the atmosphere follows a linear growth law. Tungsten and molybdenum are familiar examples of metals which generate non-protective oxides in certain environments.

The rate of oxidation of some metals may be described by a logarithmic type law, such as:

$$M = A \log (B\theta + C) \qquad (3)$$

where A, B and C are constants

The logarithmic law is less amenable to physical interpretation or theoretical development than the parabolic or linear laws. As discussed by Kubaschewski and Hopkins (3), any oxidation process which approaches a static state may be described by appropriate modifications to a law such as Eq. 3. There have been several theoretical developments of logarithmic growth laws. Evans (4) has considered the possible effects of mechanical imperfections in the oxide on the growth rate. Considering that these gross defect centers (such as blisters) act as barriers to the diffusion current, Evans stated that the rate of growth of the oxide at any time would be proportional to the oxide cross section unaffected by the defect centers. His integrated rate equation yields

an expression similar to Eq. 3. Mott and Cabrera (5) deduce a logarithmic type law in their theory of thin oxide films. They assume that the driving force for the migration of metal ions through the oxide is an electrical potential gradient. This gradient is caused by the difference between the potential of the oxygen adsorbed on the oxide surface and the potential of the metal. The potential gradient decreases with increasing oxide thickness. Eventually a static growth condition is produced when the diffusion resistance of the oxide layer balances the effect of the potential gradient. The development of protective films on aluminum and stainless steel may be described by a logarithmic law.

For some metals in a constant oxidation environment, changes in the oxidation characteristics may be observed during the course of the oxidation. For example, control of the oxidation process can shift from an interface reaction to a diffusion mechanism with increasing oxide thickness. A change in the oxidation environment can effect marked changes in the oxidation behavior. For some metals, the logarithmic growth law corresponds to low temperatures, while the parabolic and linear type laws are observed at intermediate and high temperatures, respectively. The study of the influence of gas pressure and composition on the oxidation rate has received little attention relative to the temperature factor. The extent of the pressure influence depends on the process controlling the oxidation. With a diffusion controlled oxidation, if the concentration gradient is independent of the pressure, the oxidation rate might be expected to be insensitive to

the pressure, above some limiting value. The oxidation of zinc is an example of this type.

The growth of an oxide layer requires mass transport through the oxide. For oxides such as NiO, where the ionic radius of O^{2-} is roughly twice that of the cation, it has been assumed that the principal mass flow in the oxide consists of metallic ions moving from the metal to the oxide-oxygen interface. This implies that the reaction of the metal with the oxygen occurs at the outer surface of the oxide. The present conception of the several possible mechanisms which permit mass transport through a crystal is largely based on the work of Wagner and Schottky (6) and Frenkel (7). In essence, these workers showed that various types of defect structures could provide diffusion paths through the crystal. Among the several types of defects discussed were the so-called Schottky and Frenkel defects. The Frenkel defect is characterized by a vacant lattice site and a corresponding interstitial ion or atom. Presumably both anion and cation defects of this type could occur with favorable size factors. In a Frenkel defect structure, migration of ions could occur by successive occupation of either interstitial sites or vacant lattice sites.

The Schottky defect structure is characterized by vacant lattice sites, without occupation of interstitial sites. Vacancies could occur in both the anion and the cation partial lattices. NaCl is thought to be an ionic crystal possessing vacancies in both the cation and anion lattices. Wagner and Schottky (6) showed that vacancies could be confined to the lattice of one component of the

crystal, thereby producing a deviation from the stoichiometric composition. In an ionic crystal of non-stoichiometric composition, electrical neutrality is maintained by a balancing of charge between the ions. For example, in an oxygen excess ionic crystal vacancies are confined to the cation lattice. If the normal charge for the anion is 2- and that for the cation is 2+, then for every cation vacancy there must exist two cations of charge 3+. This assumes that the favored ionic state of the anion is 2- and that further ionization of the cation (3+ to 4+) is excluded on an energy basis. The modern explanation of the effect of additives on the electrical properties of crystals is based to a considerable extent on the work initiated in Ref. (6). Several aspects of this defect theory will be discussed in connection with nickel oxide.

The work of Cairns and Ott (8) is among the first significant studies of the structure of NiO. They reported a cubic, NaCl type structure with a parameter value of 4.1768A°. Rooksby (9), using a camera of high resolution, reported that below about 200C NiO is rhombohedral. The parameters given for 18C are: $\alpha = 60^{\circ}42'$, $a = 2.9518A^{\circ}$.

The present conception of the ionic structure of NiO is based largely on electrical conductivity and thermoelectric data. Le Blanc and Sachse (10) reported a ten-fold increase in the electrical conductivity of NiO when the oxide was heated in an oxygen atmosphere. In a later work, Baumbach and Wagner (11) found the electrical conductivity to be proportional to the 1/4 power of the oxygen pressure. Their tests were conducted at 900 and 1000C,

with an oxygen pressure range of from 2×10^{-4} to 1 atm. On the basis of the dependence of the conductivity on oxygen pressure, Wagner suggested that a Schottky defect structure in the Ni^{2+} partial lattice was reasonable. The formation of this defect structure by the reaction of oxygen with the nickel ions of the lattice may be stated:

$$O_2 + 2Ni^{2+} + 4e^- \longrightarrow 2NiO + 4Ni^{3+} + 2\square Ni^{2+} \qquad (4)$$

This equation expresses the postulate that oxygen is ionized by drawing electrons from within the lattice. These electrons are taken from Ni^{2+} ions, thereby causing the transition $Ni^{2+} \rightarrow Ni^{3+}$. The Ni^{2+} ions needed to extend the lattice are taken from within the lattice, thereby creating a Ni^{2+} vacancy ($\square Ni^{2+}$) for each Ni^{2+} installed in the lattice extension. Applying the mass action principle to Eq. (4), with pO_2 the oxygen pressure:

$$\frac{[\square Ni^{2+}]^2 [Ni^{3+}]^4}{pO_2} = K \qquad (5)$$

the concentrations of the lattice electrons and the Ni^{2+} being absorbed in the constant, K. Assuming that the defect structure is created solely by the mechanism expressed by Eq. 4, then:

$$[\square Ni^{2+}] = \tfrac{1}{2}[Ni^{3+}] \qquad (6)$$

Substituting (6) into (5), the Ni^{3+} concentration may be written:

$$[Ni^{3+}] = [4KpO_2]^{1/6} = \alpha pO_2^{1/6} = \alpha pO_2^{1/n}$$

Wagner assumed a direct proportionality between the electrical conductivity and the Ni^{3+} concentration. In modern terminology, the creation of an Ni^{3+} creates a defect electron, or positive hole. Electrical conduction due solely to the motion of positive holes is designated as p-type conduction. Wagner's assumption of a predominant p-type conductivity has been substantiated by subsequent work, to be discussed. The electrical conductivity may then be expressed:

$$\sigma = a[Ni^{3+}] = apO_2^{1/6} = apO_2^{1/n} \qquad (7)$$

As mentioned above, Baumbach and Wagner found that the conductivity was proportional to the 1/4 power of the oxygen pressure, i.e., n equals 4 on the basis of these data. Considering that concentrations, rather than activities, were used in the mass action expression leading to Eq. 7, the agreement between the experimental and predicted values of n is in fair support of the defect model.

The assumption that normal NiO has a Schottky defect structure in the nickel partial lattice implies that NiO is a metal deficit oxide. Chemical analysis has shown that NiO <u>does</u> exist with a metal deficiency with respect to the formula NiO. Some oxygen excess data will be discussed later.

The thermoelectric power data obtained from the coupling metal-oxide-metal may be used to determine the character of the current carriers in a material such as NiO. Hogarth (12) has found that thermoelectric power data for several oxides, including

NiO, follow the empirical formula:

$$\frac{dE}{dT} = C \log (pO_2) + \text{const} \qquad (8)$$

where dE/dT is the thermoelectric power (volts/degree). By applying semi-conductor theory to the metal-oxide-metal coupling, Hogarth obtained the following expression for C in Eq. 8:

$$C = \frac{k}{en}$$

where k is Boltzmann's constant, e is the value of the charge on the current carrier, and n is the denominator of the exponent in Eq. 7. The thermoelectric power (dE/dT) is positive for a p-type conductor and negative for an n-type, regular electron, conductor, thus permitting a determination of the type of conduction prevailing in the oxide. dE/dT was found to be positive for NiO, thus confirming the p-type conduction. In addition, Hogarth obtained a value of n equal to 4.8, using thermoelectric data obtained by Baumbach and Wagner for NiO. This value for n is in slightly better agreement with the value of 6 predicted by the defect model.

Recently, Morin (13) obtained additional confirmation of the p-type conduction in NiO using the thermoelectric technique. In addition, Morin attempted to obtain a value of the Hall coefficient for NiO, using both powdered and single crystal specimens. The Hall voltage could not be detected for either the powdered or the single crystal specimens, indicating a very low mobility for the current carriers in NiO. Morin estimated the carrier mobility to be less than 0.1cm /volt sec. This low mobility of the positive

holes in NiO was first suggested by DeBoer and Verwey (14) in their consideration of the most probable ionic structure for NiO. The details of the several energy models which have been offered in explanation of the low carrier mobility in NiO are not of direct interest to this discussion. In summary of the above discussion of pure NiO, the work discussed has established NiO as a metal deficit, p-type semi-conductor.

The discussion of the introduction of foreign ions to the NiO lattice will be confined principally to chromium. When the concentration of chromium is low relative to the concentration of defects associated with the pure NiO ($\square Ni^{2+}$ and Ni^{3+}), one possible method of chromium addition may be expressed:

$$\tfrac{1}{2}O_2 + \square Ni^{2+} + Ni^{3+} + Cr \rightarrow Cr^{3+} + O^{2-} + Ni^{2+} \qquad (9)$$

This equation expresses the postulate that the first chromium ions are installed in vacant sites associated with the pure NiO. The chromium is ionized partially at the expense of the Ni^{3+}, causing the transition $Ni^{3+} \rightarrow Ni^{2+}$. Thus, according to Eq. 9, for every chromium ion added, one nickel vacancy and one Ni^{3+} are destroyed. It is to be noted that on the basis of the vacancy diffusion mechanism, chromium addition according to Eq. 9 would be expected to <u>decrease</u> the oxidation rate. There are other possible reactions of chromium with the NiO lattice which will be discussed later. In a recent study of the effect of additives on the electrical properties of NiO, Parravano (15) obtained partial confirmation of the above model. Using a thermoelectric method initiated by Morin (13), Parravano

related the thermoelectric power to the concentration of positive holes ($\rightarrow [Ni^{3+}]$) in NiO containing various additives. The pertinent equations are:

$$QT = E_F \tag{10}$$

$$p = N \exp(-E_F/kT) \tag{11}$$

where $E_F >> kT$.

Q is the thermoelectric power, T is the absolute temperature, E_f is the difference between the Fermi level and the filled d levels of Ni^{2+}, p is the concentration of holes and N is the concentration of nickel atoms ($5.6 \times 10^{22} cm^{-3}$). By measuring the thermoelectric power Q and thus finding E_f, the hole concentration may be found from Eq. 11. Parravano compared the hole concentration found with a given additive concentration to the hole concentration found for pure NiO. The increase, or decrease of holes per additive atom could thus be determined. Assuming a correspondence between the number of holes and the number of additive atoms, the concentration of the additive can be determined from the thermoelectric data. Morin (13) had previously found good agreement between the concentration of lithium additions in NiO determined chemically and by the thermoelectric method. Parravano found good agreement between chemically and thermoelectrically determined concentrations for silver, lithium and chromium. The addition of a singly charged ion, such as Li^{1+}, may be written:

$$\tfrac{1}{2}O_2 + Li + Ni^{2+} \rightarrow O^{2-} + Li^{1+} + Ni^{3+} \tag{12}$$

related the thermoelectric power to the concentration of positive holes ($\rightarrow [Ni^{3+}]$) in NiO containing various additives. The pertinent equations are:

$$QT = E_F \tag{10}$$

$$p = N \exp(-E_F/kT) \tag{11}$$

where $E_F >> kT$.

Q is the thermoelectric power, T is the absolute temperature, E_f is the difference between the Fermi level and the filled d levels of Ni^{2+}, p is the concentration of holes and N is the concentration of nickel atoms ($5.6 \times 10^{22} cm^{-3}$). By measuring the thermoelectric power Q and thus finding E_f, the hole concentration may be found from Eq. 11. Parravano compared the hole concentration found with a given additive concentration to the hole concentration found for pure NiO. The increase, or decrease of holes per additive atom could thus be determined. Assuming a correspondence between the number of holes and the number of additive atoms, the concentration of the additive can be determined from the thermoelectric data. Morin (13) had previously found good agreement between the concentration of lithium additions in NiO determined chemically and by the thermoelectric method. Parravano found good agreement between chemically and thermoelectrically determined concentrations for silver, lithium and chromium. The addition of a singly charged ion, such as Li^{1+}, may be written:

$$\tfrac{1}{2}O_2 + Li + Ni^{2+} \rightarrow O^{2-} + Li^{1+} + Ni^{3+} \tag{12}$$

Here the addition of one Li^{1+} involves the creation of one Ni^{3+}. This is in contrast to the chromium addition according to Eq. 9, where one Ni^{3+} is destroyed for each Cr^{3+}. Eq. 12 implies that the lithium addition produces an extension of the lattice, i.e., involves oxygen. Another possible method of Li addition does not involve lattice extension and will be discussed later. Parravano found roughly a 1:1 ratio between the number of additive atoms and the number of holes created for silver and lithium. For chromium additions, he also found a near 1:1 ratio between the number of chromium ions added and the number of holes destroyed.

If the concentration of chromium in the oxide is much greater than the concentration of defects associated with the pure NiO, the addition of chromium is thought to occur as follows:

$$\frac{3}{2} O_2 + 2\,Cr \rightarrow 3O^{2-} + 2\,Cr^{3+} + 1\,\square Ni^{2+} \qquad (13)$$

Here a nickel vacancy is created for every two chromium ions added to the lattice. This process presumably could continue until some saturation concentration of chromium in NiO is reached. According to Eq. 13, the nickel vacancy concentration is one half the chromium concentration. Assuming that diffusion through the NiO occurs via the cationic vacancies, and that the oxidation process is diffusion controlled, then the oxidation rate would be expected to increase with chromium addition. This increase in oxidation rate with chromium addition would persist until a saturation

of chromium in the NiO produced a new phase, or phases, in addition to the NiO. These new phases could be expected to alter the diffusion rate through the oxide layer, thereby effecting a gradual, or abrupt, change in the rate of increase of oxidation rate with chromium addition. Horn (16) and Wager and Zimens (17) obtained oxidation data for Ni-Cr alloys at 900 and 1000C, respectively. The oxidation rate-At°/o chromium relationship obtained by these workers showed the expected increase in oxidation rate with chromium addition up to roughly 10At°/o chromium. With greater chromium additions, tney observed a rapid decline in oxidation rate. Assuming the cationic vacancy diffusion mechanism is applicable to the nickel-chromium mixed oxide, these data are in support of the defect model expressed by Eq. 13.

Chromium addition in NiO according to Eq. 13 might be expected to decrease the lattice parameter of NiO. The Goldschmidt radii for Cr^{3+} and Ni^{2+} are 0.64 and 0.70A°, respectively. The Cr^{3+} for Ni^{2+} substitution could not be expected to increase the parameter. In addition there is a reasonable possibility that an increase in the vacancy content will reduce the parameter, since a decrease in lattice parameter with vacancy increase has been noted for FeO (18) and TiO (19). Both FeO and TiO have the NaCl structure and both can exist with a metal deficiency--in common with NiO. FeO and TiO showed a nearly linear decrease in parameter with oxygen excess (vacancy increase). Apparently there has been no work on the effect of chromium additions on the NiO lattice parameter. If a correspondence is assumed between the lattice

of chromium in the NiO produced a new phase, or phases, in addition to the NiO. These new phases could be expected to alter the diffusion rate through the oxide layer, thereby effecting a gradual, or abrupt, change in the rate of increase of oxidation rate with chromium addition. Horn (16) and Wager and Zimens (17) obtained oxidation data for Ni-Cr alloys at 900 and 1000C, respectively. The oxidation rate-At°/o chromium relationship obtained by these workers showed the expected increase in oxidation rate with chromium addition up to roughly 10At°/o chromium. With greater chromium additions, tney observed a rapid decline in oxidation rate. Assuming the cationic vacancy diffusion mechanism is applicable to the nickel-chromium mixed oxide, these data are in support of the defect model expressed by Eq. 13.

Chromium addition in NiO according to Eq. 13 might be expected to decrease the lattice parameter of NiO. The Goldschmidt radii for Cr^{3+} and Ni^{2+} are 0.64 and 0.70A°, respectively. The Cr^{3+} for Ni^{2+} substitution could not be expected to increase the parameter. In addition there is a reasonable possibility that an increase in the vacancy content will reduce the parameter, since a decrease in lattice parameter with vacancy increase has been noted for FeO (18) and TiO (19). Both FeO and TiO have the NaCl structure and both can exist with a metal deficiency--in common with NiO. FeO and TiO showed a nearly linear decrease in parameter with oxygen excess (vacancy increase). Apparently there has been no work on the effect of chromium additions on the NiO lattice parameter. If a correspondence is assumed between the lattice

parameter and the amount of chromium installed in the NiO, then lattice parameter data should provide a check on the applicability of the nickel-chromium mixed oxide defect model to the oxidation of nickel-chromium alloys.

There is yet substantial ignorance concerning the limit of chromium solubility in the NiO lattice and the disposition of the chromium once the solubility limit has been reached. The present limited knowledge of mixed oxides also permits some doubt concerning the dominance of the cationic vacancy diffusion mechanism over wide ranges of the oxide omposition. These factors are of obvious importance in the oxidation process of nickel-chromium alloys.

III. EXPERIMENTAL PROCEDURE FOR OXIDATION

There are three principal techniques employed for securing oxidation rate data, namely: the manometric method, wherein the rate of pressure decrease in a closed system is directly related to the rate of oxidation; the continuous, or semi-continuous weighing method in which the specimen is coupled directly to a weighing device throughout the oxidation period; the discontinuous weighing method, wherein different specimens are exposed for the desired time increments and the weighing is done before and after introduction to the furnace. Of the three methods, the continuous weighing and manometric methods obviously permit the best resolution of the weight gain-time relationship. Gensch and Hauffe (20) employed the manometric technique in a study of the oxidation of zinc alloys. Gulbransen (21) has employed a quartz microbalance of high sensitivity to obtain semi-continuous weight gain-time relationships of great detail. In the present work, it was most expedient to use the discontinuous weighing method. Apart from the lack of detail in the weight gain-time relationship, the principal objection to the discontinuous weighing method is that specimen manipulation may cause loss of the oxide. With techniques permitting the use of a single specimen, however, multiple tests are still desirable to properly average possible physical errors and deviations due to specimen nonuniformity.

A. Apparatus

The basic oxidation system is sketched in Fig. 1. Oxygen from the high pressure supply was given primary pressure re-

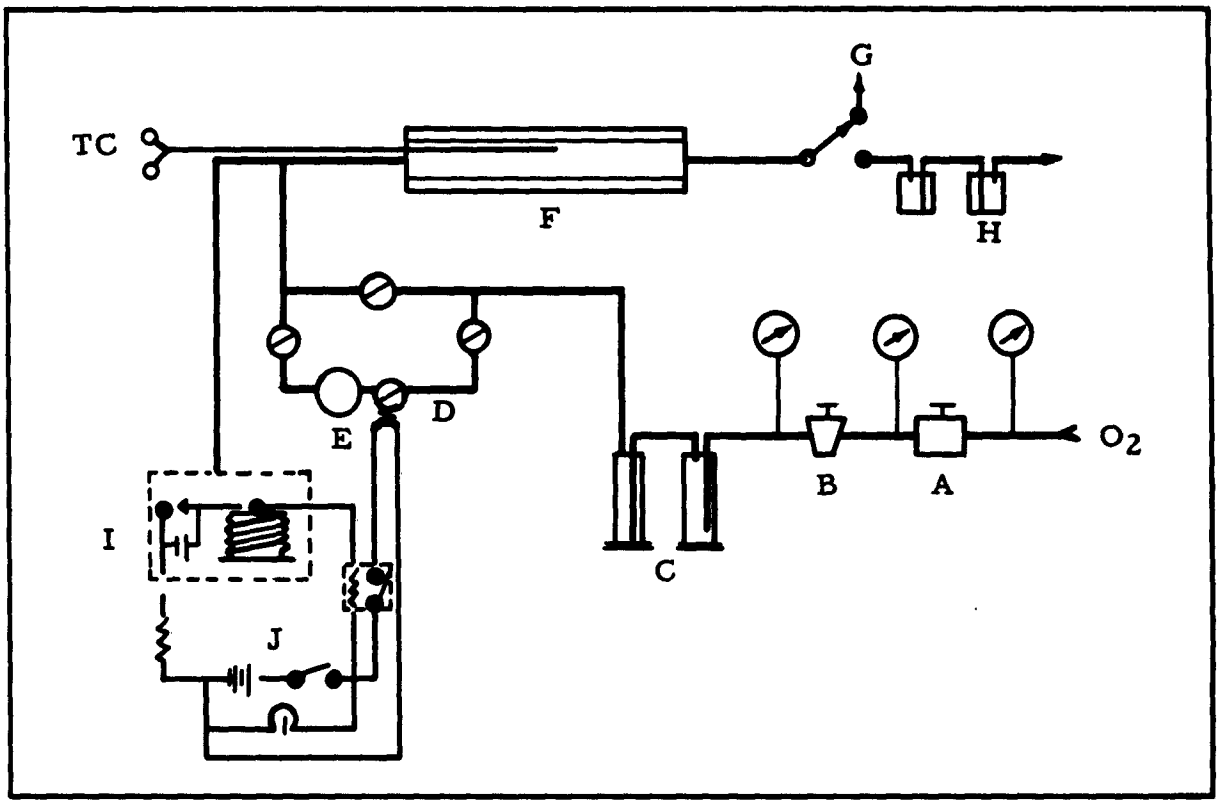

A - step down reg.
B - precision reg.
C - P_2O_5 driers
D - solenoid valve
E - reservoir
F - furnace
G - fast vent
H - H_2SO_4 bubbler
I - microbarograph
J - barostat circuit

Fig. 1

Oxidation Apparatus

duction by a Grove regulator (A), then secondary reduction by a Moore precision regulator (B). The gas was led through two P_2O_5 driers and then to a barostat circuit, or directly through the by-pass valve to the furnace. The barostat system consisted of a microbarograph (I) and a relay circuit (J) which controlled a solenoid valve (D). Although the barostat gave a satisfactory stability, the performance of the precision regulator was such that only occasional manual adjustment gave the desired pressure control. The regulator maintained the test pressure to within ± 0.1 cm at 76 cm Hg. A Burrell high temperature furnace was used. The zirconium oxide furnace tube was provided with an interior quartz oxidation tube, fitted with a ground joint at one end. A chromel-alumel control thermocouple, periodically replaced, was led to within one inch of the center of the specimen. The thermocouple junction was coated with Sauereisen cement to extend the operating life. Temperature control was provided by a Leeds and Northrup Micromax controller. The oxidation zone was checked for temperature uniformity and the gradient was found to be less than $0.5^{\circ}C\ cm^{-1}$ over the oxidation zone. It is estimated that the temperature of the specimen was held to within $\pm\ 6^{\circ}C$ of the test temperature 1096C. The gas was led from the furnace to a selector valve, which provided either a quick vent for flushing or a slow vent through a trap and H_2SO_4 bubbler. The latter was used for the tests and a bubble rate of about 3 per second was maintained throughout the tests.

Prior to a test, the system was flushed with oxygen for

about 15 minutes. Preceding and during the flushing, the furnace was brought to the test temperature. With the furnace at the control point, the quartz oxidation tube was opened and the specimen placed in the oxidation zone as quickly as possible. The operation of placing the specimen and resealing the tube could be performed in 10-15 seconds. With the specimen in position, the test pressure was quickly established. Tests of the heating and cooling rates of the specimens showed that the correction to the control temperature to compensate for heating and cooling periods was within the limits of error of the control. An electric timer was actuated by a switch at the furnace. At the conclusion of a test, the specimen was quickly removed and placed in a desiccator to cool to room temperature. Cooling was accelerated by a stream of argon through the desiccator.

B. Oxygen

Aviators' breathing-oxygen was used for this work. Purity specifications for this gas state that the oxygen content is to exceed 99.5%, with a water vapor content not to exceed 0.035 mg/liter. Nitrogen is listed as the principal impurity. Other than the use of several P_2O_5 traps for water vapor, no attempt was made at further gas purification.

C. Material for Oxidation

The high sensitivity of the oxidation rate of nickel to impurities is indicated by the wide variation in oxidation rates reported by various workers for nickel. In order to properly identify the effects of chromium additions, it was mandatory to secure oxidation material of high purity. A series of nickel-chromium

alloys varying from pure nickel to about 11At°/o chromium was purchased from Battelle Memorial Institute. Chemical and spectographic analysis showed that the impurity aggregate averaged less than 0.1°/o for this material. Silicon, iron and zinc were the principal impurities. Battelle employed high purity Baker shot nickel and iodide chromium, made at Battelle, as the components for this material. Melting was done in a vacuum induction furnace. The ingots were cold rolled, with intermediate vacuum annealing when necessary. Several additional alloys were prepared at this laboratory, extending the chromium content to 16.5At°/o. For this latter material the high chromium Battelle material was supplemented with hydrogen reduced chromium powder. Melting was done in an arc furnace under a helium atmosphere. The ingots were cold rolled to size, without intermediate annealing.

All alloy specimens were rough cut from the sheet stock and milled or filed to the desired rectangular shape. For the bulk of the test work, the specimen area was about $10cm^2$, with an average thickness of about 0.05 cm. When material shortage prohibited the use of large specimens, a specimen of about $2.5cm^2$ area was used. The thickness of 0.05 cm was held for all specimens. The specimen dimensions were obtained with a Bausch and Lomb Contour Comparator, used at 10X, and with micrometers. When it became apparent that the oxidation data scatter was not significantly reduced by employing the comparator, all measurements were made with micrometer gauges. Weight measurements were made with an Oertling microbalance.

D. Atmospheric Oxidation

Because of the unavoidable interval between the first weighing and the oxidation, it was of interest to measure the weight change of a freshly polished specimen, exposed to the air over a period of several days. One sample of 100°/o nickel and one of about 6 At°/o chromium were electropolished and stored under absolute alcohol until the first weighing. The interval between drying and the first weighing was of the order of 10 minutes. Weighings were made at hourly intervals for a period of four hours, and then at 24 hour intervals for three days. Over the total test period, the 100°/o nickel specimen showed a weight loss of 0.000002 gm. The 6°/o chromium alloy showed a loss of 0.000008 gm. These weight changes cannot be considered significant considering the test conditions. In view of the attention to thick oxide films in the present work no attempt was made to correct for, or to remove, the atmospheric oxidation.

E. Pre-oxidation Grain Size and Surface Preparation

In order to minimize the grain boundary diffusion, a large grain size was obtained for the oxidation material by a vacuum anneal at 1260C for 24 hours. The resulting grain size proved uniform for all alloys. A typical section is shown in Fig. 2. Subsequent to the anneal, the specimens were abraded through 600 paper. This mechanical polish was followed by an electropolish in a sulfuric acid-glycerol bath. The polish was conducted at 70 C, 0.15 amps cm^2, for 6 minutes. Subsequent treatment consisted of a soap wash followed by water and absolute alcohol rinses.

F. Specimen Manipulation

It was initially planned to expose specimens of each alloy simultaneously. Accordingly, a quartz frame was made to permit the admission of 8-10 specimens to the furnace simultaneously. This technique proved satisfactory for the commercial nickel tests, discussed later. It was observed, however, that the quench-cracking of the nickel-chromium oxides was severe. Accordingly, each specimen was oxidized within its own quartz capsule. The capsule was provided with a loosely fitting cap at one end and a small hole at the other to insure free oxygen circulation with containment of the oxide. This technique limited simultaneous exposure to a maximum of four specimens. The capsules were mounted in a nickel or nichrome boat, manipulated by a quartz pull rod. This procedure was also used for the high purity nickel material, although it exhibited no quench-cracking. The blistering occasionally observed on the pure nickel is shown in Fig. 3. A typical quench cracked nickel-chromium oxide is shown in Fig. 4.

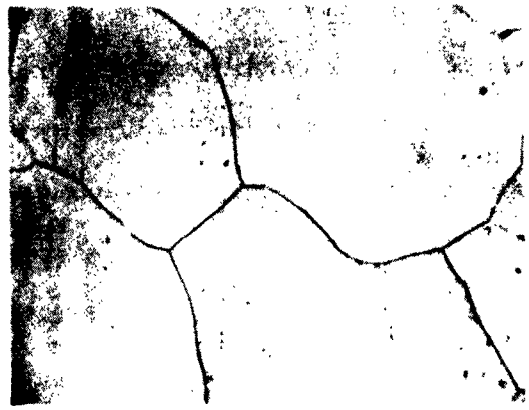

Fig. 2

Typical Pre-Oxidation Grain Size (Alloy 6)
(100X)

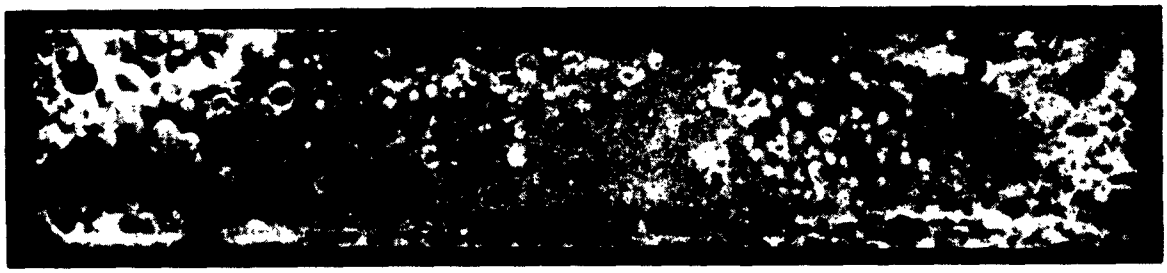

Fig. 3

Blisters on 100% Nickel Specimen After One Hour Oxidation
(3X)

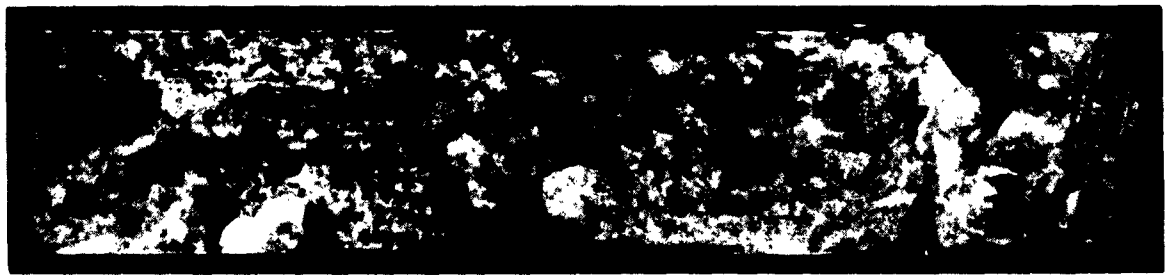

Fig. 4

Typical Quench Cracking of Oxide for Ni-Cr Alloys
(3X)

IV. OXIDATION RESULTS

A. Surface Treatment Effects

The effects of surface condition on the oxidation rate has received somewhat cursory attention from many workers. Apparently there has not appeared a quantitative analysis of this important aspect of the metal-oxygen reaction. Gulbransen and Andrews (22) conducted oxidation tests on high purity nickel which had received several different surface treatments. Among the treatments considered were: abrasion through 4/0 paper; electropolishing, followed by a hydrogen anneal at 900 C for 12 hours. Specimens mechanically polished through 4/0 paper exhibited a significantly lower oxidation rate than electropolished specimens, after about 0.3 hour of oxidation. Tests apparently were conducted at 600 C under 7.6 cm Hg of oxygen. The two sets of data continued to diverge out to the 2 hour time limit of the testing. At the test limit, M^2 ($gm^2 cm^{-4}$) for the electropolished material was roughly 60% greater than the M^2 value for the mechanically polished material.

It was desired to test the effects of mechanical and electropolishing on the oxidation rate, for the environment and exposure interval pertinent to this work. Accordingly, two groups of specimens were prepared from commercial nickel sheet (98.5% nickel, ASTM grain size 5). One group received mechanical polishing through 600 paper, the other group was given the same abrasion, followed by electropolishing, as described above. The oxidation rate data for these materials are given

Table 1

Oxidation Data for Mechanically Polished and Electropolished Commercial Nickel

1096C 76 cm Hg of O_2

Spec.	θ (secs)	M^2 (gm^2cm^{-4})	K_p ($gm^2cm^{-4}sec^{-1}$)
1 EP	3640	4.43×10^{-6}	12.2×10^{-10}
1 MP	3640	4.29×10^{-6}	11.8×10^{-10}
2 EP	7330	9.70×10^{-6}	13.2×10^{-10}
2 MP	7330	9.76×10^{-6}	13.3×10^{-10}
3 EP	14490	19.3×10^{-6}	13.3×10^{-10}
3 MP	14490	18.4×10^{-6}	12.7×10^{-10}
4 EP	28910	35.2×10^{-6}	12.2×10^{-10}
4 MP	28910	38.4×10^{-6}	13.3×10^{-10}

$\bar{K}_p$ for electropolished material (EP) : 12.7×10^{-10}

$\bar{K}_p$ for mechanically polished material (MP) : 12.8×10^{-10}

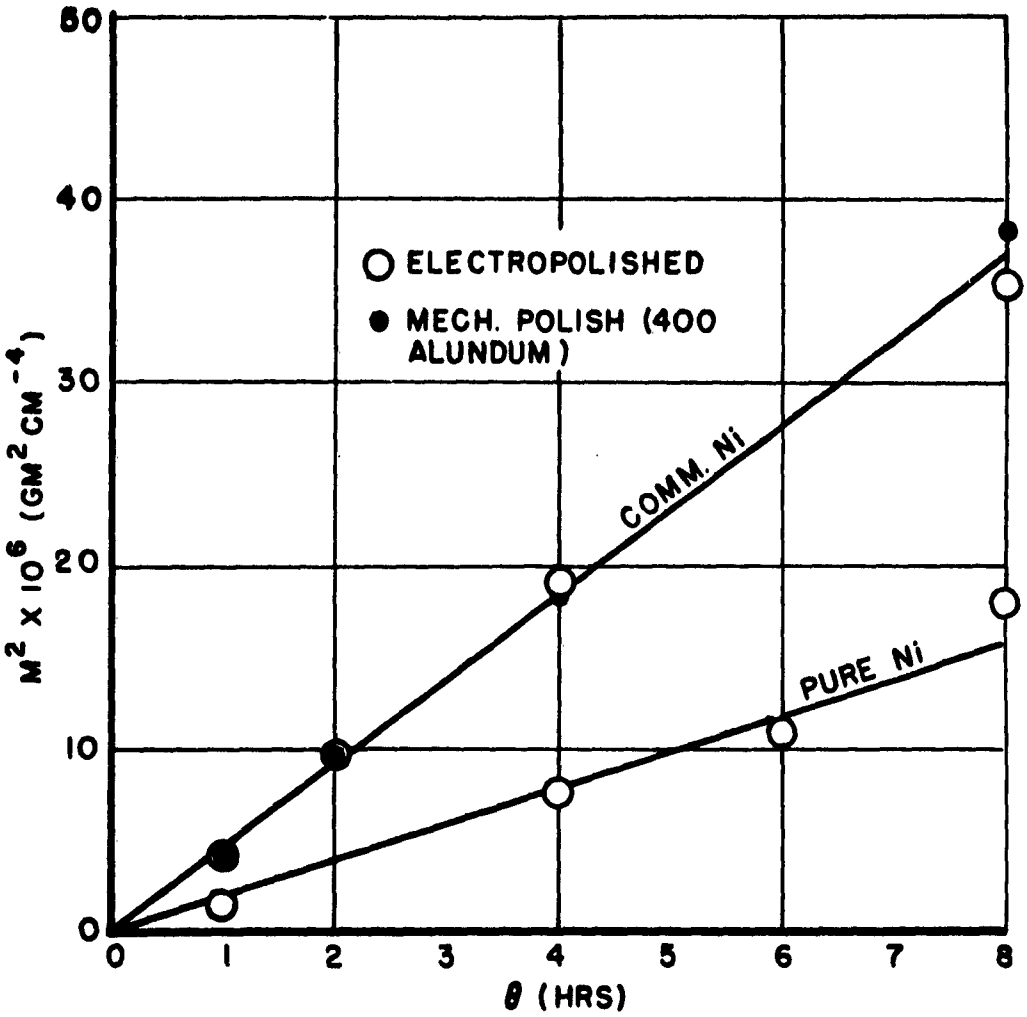

Fig. 5
M^2-θ Characteristic for Commercial Nickel and High Purity Nickel

1096°C
76cm Hg of O_2

in Table 1, and the M^2-θ characteristic is plotted in Fig. 5. Within the limits of experimental error no significant difference in oxidation rate could be detected for the two surface treatments. The slopes of the separate curves (only the arithmetic mean of the two sets of data is plotted), yielded parabolic rate constants which were remarkably close. These results are in disagreement with the work of Gulbransen and Andrew, obtained with high purity material and at a lower temperature and pressure. The hydrogen anneal given the electropolished specimens complicates the comparison between the present data and those of Gulbransen and Andrew. Similar comparison tests were not made with the high purity material. All oxidation work with the high purity material was done with electropolished specimens. Uhlig and Brenner (23) suggest that mechanical filing yields the highest surface reproducibility. Mechanical working of a surface layer certainly does not contribute to a uniform grain size throughout the specimen, at the test temperatures of this work. A brief discussion of some effects of cold work on the oxidation rate is given later.

B. Oxidation of High Purity Nickel

The oxidation rate of high purity nickel serves as a logical reference for the nickel-chromium alloys. Gulbransen and Andrew (22) and Kubaschewski and Hopkins (3) have summarized the oxidation data for nickel of various degrees of purity and over a range of temperatures. The sensitivity of the oxidation rate to impurity content is evident from the remarkable spread in the log parabolic rate constant-1/T relationships reported

by various workers. The nickel used by Gulbransen and Andrew and that used in this study was of comparable purity (>99.95% after vacuum annealing). Gulbransen and Andrew reported rate data for 550, 600, 625, 650 and 700C, under 7.6 cm Hg of oxygen. In addition to the tests to establish the oxidation rate at 1096C, pure nickel rate data were obtained at 980 and 1260C, under 76 cm Hg of oxygen. The M^2-θ characteristic, obtained at 1096C for the high purity nickel, is given in Fig. 5. The parabolic rate constants for 980 and 1260C were obtained by an arithmetic average of the results of four exposures of six hours each, for each temperature. Average deviations from the reported rate constants were 15% and 8% for the 980 and 1260C data, respectively.

The data from the two sources are tabulated in Table 2. Log K_p is given as a function of 1/T in Fig. 6. There is good agreement between the low temperature rate data of Gulbransen and Andrew and the present high temperature data. The insensitivity of the oxidation rate to a tenfold increase in the oxygen pressure is noteworthy. This pressure independence, above some limiting value, has been observed for many materials. Moore (24) suggests 10 cm Hg of oxygen as an approximate pressure limit for nickel. The continuity between Gulbransen and Andrew's data and the present data supports the existence of a pressure independence limit somewhat less than 7.6 cm Hg. Gulbransen and Andrew reported an activation energy of 41.2 K cal/mole on the basis of their data. Applying a method of

Table 2

Oxidation Data For High Purity Nickel (> 99.95%)

pO_2 (cmHg)	T (°C)	K_p ($gm^2 cm^{-4} sec^{-1}$)	Source
7.6	550	1.08×10^{-14}	Ref. 22
7.6	600	5.23×10^{-14}	Ref. 22
7.6	625	6.83×10^{-14}	Ref. 22
7.6	650	1.46×10^{-13}	Ref. 22
7.6	700	5.08×10^{-13}	Ref. 22
76	980	1.14×10^{-10}	Present work
76	1096	5.48×10^{-10}	Present work
76	1260	34.1×10^{-10}	Present work

averages analysis to the combined data, shown in Fig. 6, an activation energy of 45.1 Kcal/mole was obtained.

The nickel oxide obtained at 980 and 1096C exhibited a dull greenish-black outer surface and a light green substructure. This color variation had been noted by Pilling and Bedworth (2), among other workers. The outer surface of the 1260C oxide was noticeably darker in color and more glossy than the low temperature oxides. The dark modifications of the usual light green nickel oxide are thought to be attributable to an oxygen excess. Le Blanc and Sachse (25) and Cairns and Ott (8) dispelled the earlier concept that the black oxide was another compound by X-ray studies which showed that the black modifications gave the NiO pattern. The oxide generated at all the test temperatures proved to be exceedingly adherent. Specimens of the oxide were most easily removed by vigorous application of a diamond scriber. The oxides formed on the commercial nickel and the high purity nickel showed no evidence of quench cracking, in marked contrast to the nickel-chromium oxides. Photomicrographs of the outer surface of the 1096C and 1260C oxides are given in Figs. 7 and 8. A stepwise growth and rather random orientation of the NiO crystals is evident for the 1096C oxide. The 1260C oxide, after six hours exposure, showed only a very flat surface of massive NiO crystals. Under high magnification, the formation of new crystals on both the 111 and 100 planes was clearly evident. This secondary growth was only observed for the 1260C oxide.

The phenomenon of blistering during oxidation has been

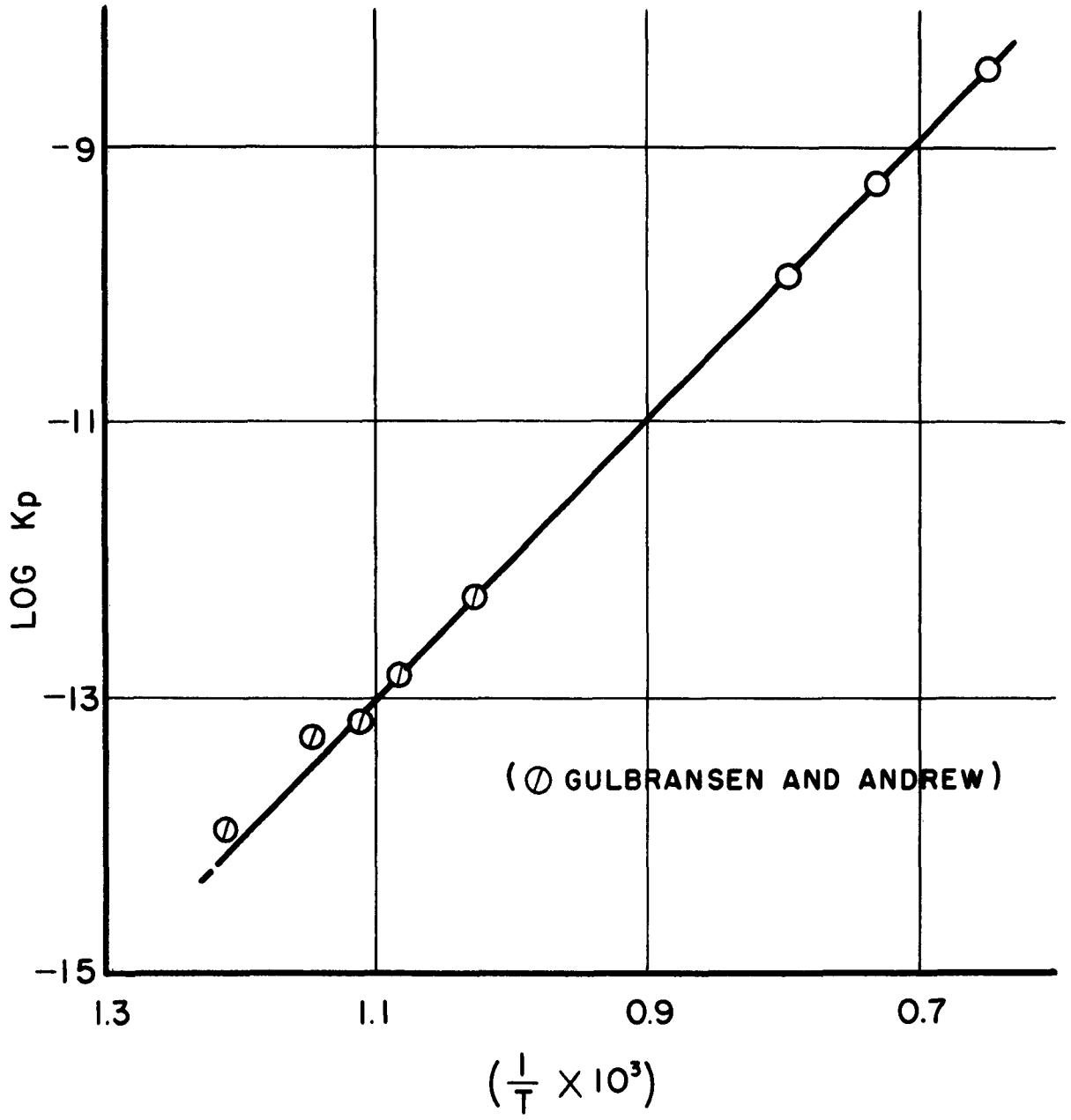

Fig: 6

Log K_p vs. 1/T

For
High Purity Nickel

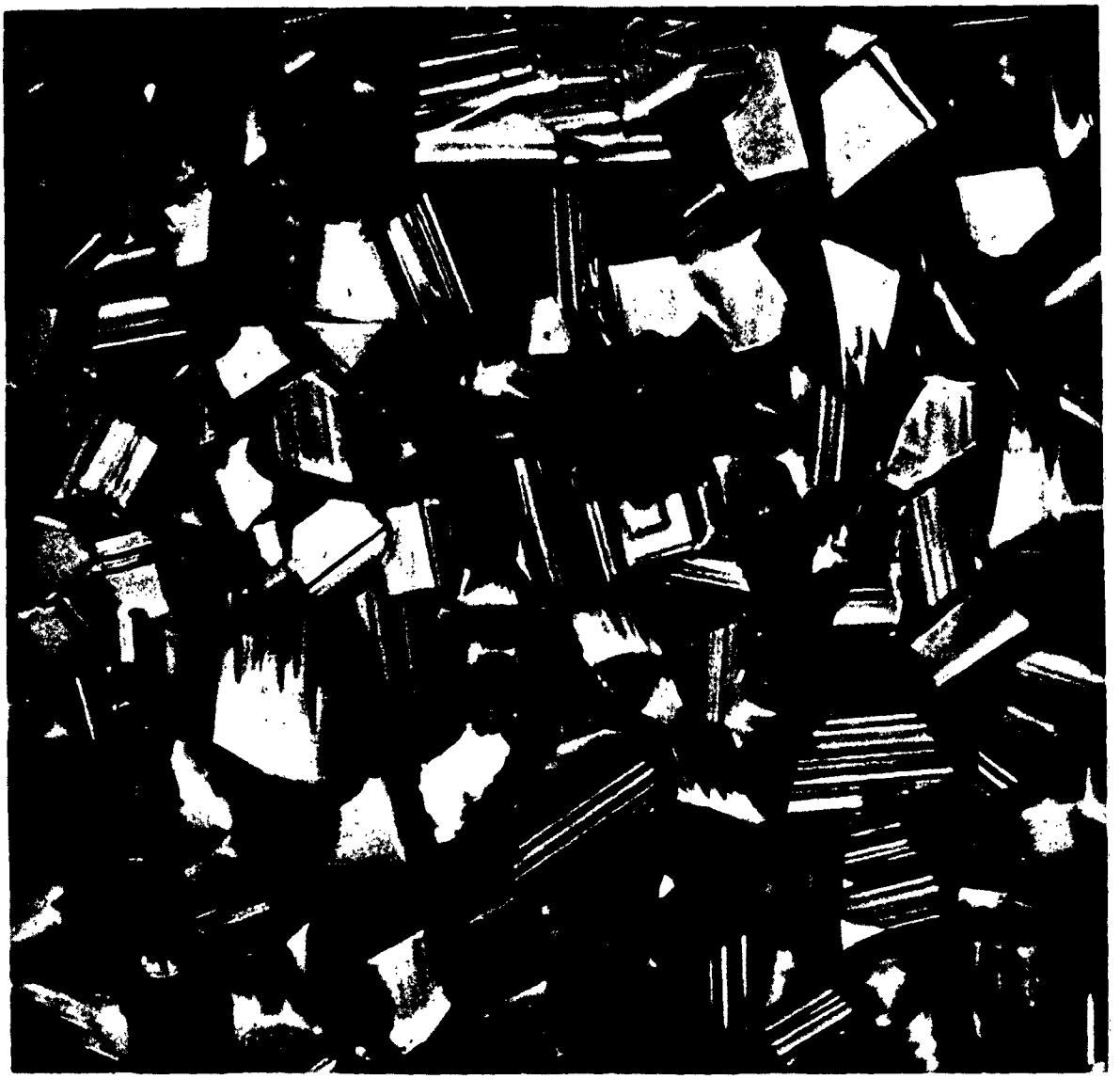

Fig: 7

Oxide Formed on 99.95% Nickel

1096°C
76 cm Hg of O_2
Six Hours Exposure

(700X-enlarged 2X)

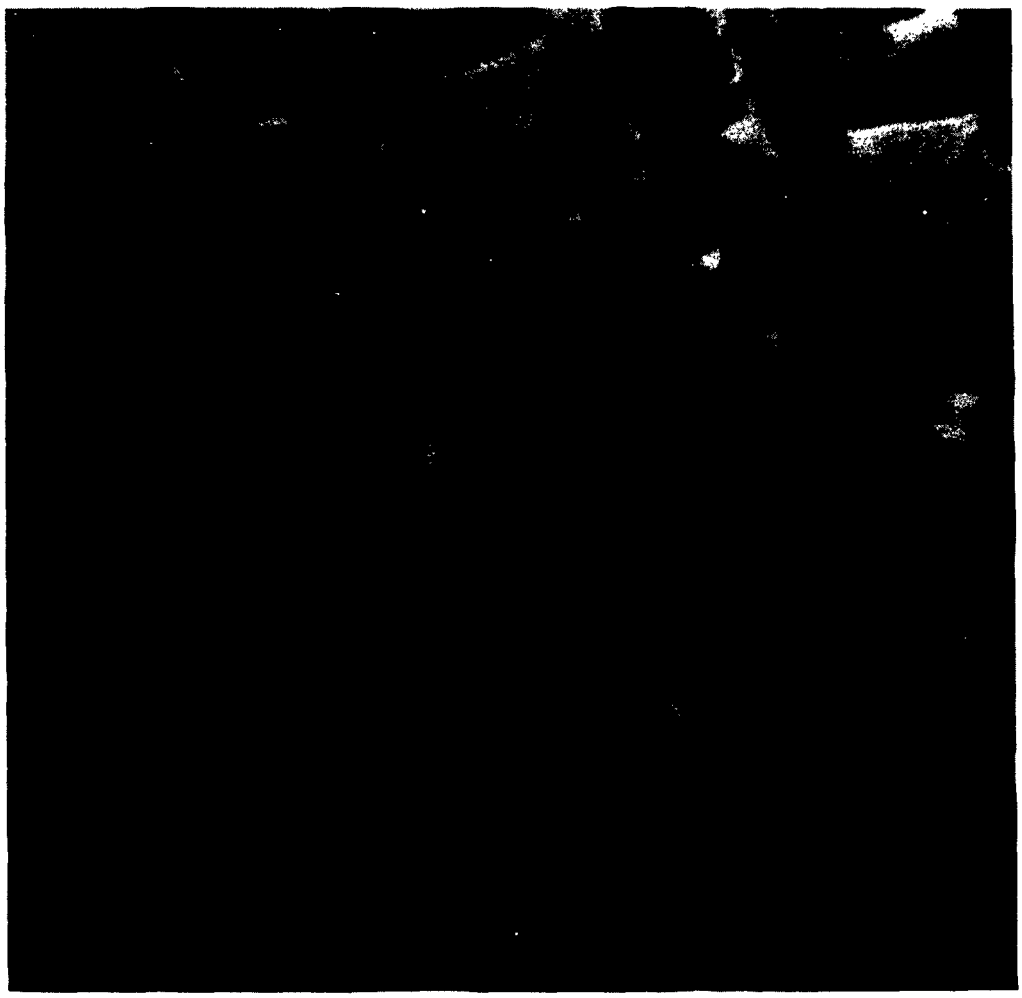

Fig: 8

Oxide Formed on 99.95% Nickel

1260° C
76 cm Hg of O_2
Six Hours Exposure

(2000X-enlarged 1.5X)

observed for many metals. Several pure nickel specimens oxidized at 980C and 1096C exhibited blisters of various sizes. A typical blistered specimen was shown in Fig. 3. When the specimen showed evidence of blistering, the test was repeated. Fortunately, the incidence of blistering was low for the high purity material. The commercial nickel showed no blistering with either the abraded or the electropolished surfaces. The mechanical and chemical factors effecting blistering are not yet established. Time did not permit a closer examination of this interesting, if troublesome, phenomenon.

C. Oxidation of Nickel with Chromium Additions

As mentioned earlier, because of the severe quench cracking exhibited by the nickel-chromium oxides, it was necessary to provide a quartz capsule for each specimen. The cracking of the oxide during cooling was barely perceptible for the lowest chromium alloy (0.36At°/o chromium) and increased in severity with chromium addition. The outer surface of the high chromium oxides was almost completely removed by cooling of the oxide-metal compact to room temperature. The inception and progression of the oxide cracking could be clearly observed through the quartz. Cracking was not noticed until the specimen had cooled below a visible heat color ($\sim$ 700C). Fragments of the oxide were observed to separate with considerable violence.

The oxides generated by all the nickel-chromium alloys of this study had several common structural features. With the exception of the highest chromium alloy (16.5At°/o), the outer surface was composed entirely of large NiO crystals of greenish

black color. No significant change in crystal size, or color, with chromium content was observed. The stepwise growth evident for the pure nickel (Fig. 7) was not noticed for alloys of greater than 0.36At°/o chromium content. With increased chromium addition, the outer NiO crystals appeared to present greater irregularity in development perpendicular to the surface of the specimen. This is somewhat evident in the photomicrographs taken of alloys 1-6 at 100X and 700X after six hours exposure (Figs. 9 and 10). The large metal grains appeared to have some influence on the oxide growth for the pure nickel and 0.36At°/o chromium alloy. Slight differences in orientation of the NiO crystals delineated a pattern which appeared to be a copy of the metal grain pattern. The fine lines observed in Fig. 9 on the pure nickel and 0.36At°/o chromium oxides could be quench cracks or evidence of metal grain boundary effect on the oxidation rate. The highest chromium alloy tested (16.5At°/o) exhibited a discontinuous field of large NiO crystals on the surface. The intermediate regions (identified as Cr_2O_3 by X-rays) were composed of extremely small crystallites, barely resolvable at 2000X. A typical composite area of this oxide is shown in Fig. 11. One of the prominent Cr_2O_3 regions is shown in greater detail in Fig. 12.

A second physical feature of the oxide layer, common to all the nickel-chromium alloys, was a substrate of almost powdery consistency which extended to the metal. The substrate color varied from blue green or dark green adjacent to the outer layer of massive NiO crystals to a light greenish-brown near the metal. It was also observed that the substrate was less adherent to the

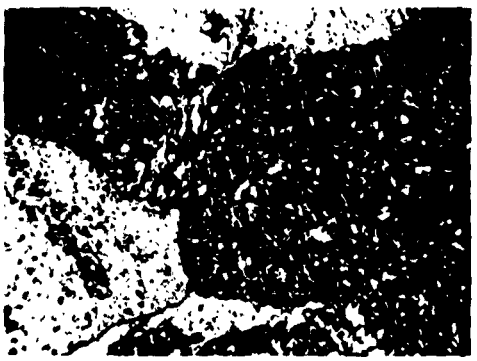

100% Ni

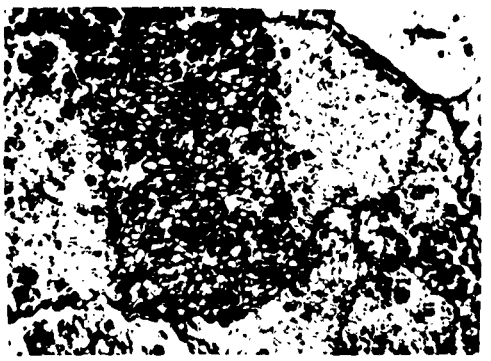

0.36 At% Cr

1.04 At% Cr

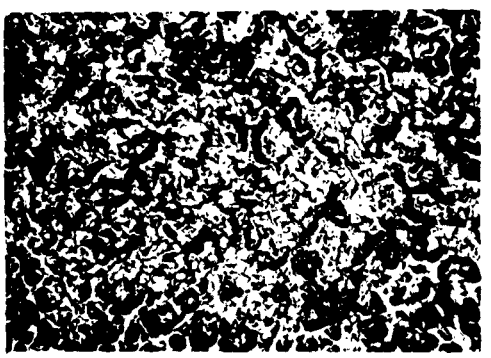

2.25 At% Cr

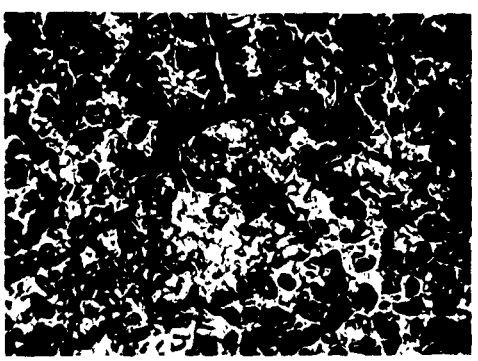

3.88 At% Cr

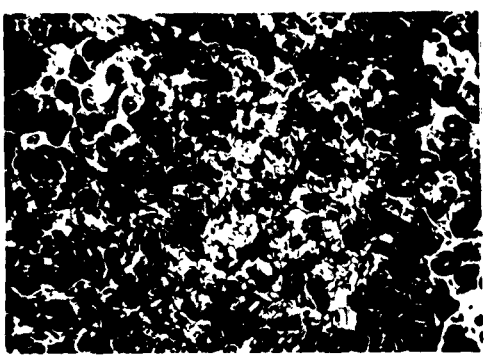

6.37 At% Cr

Fig: 9

Outer Oxide Surface
Six Hours Oxidation
(100X)

100°/o Ni

0.36 At°/o Cr

1.04 At°/o Cr

2.25 At°/o Cr

3.88 At°/o Cr

6.37 At°/o Cr

Fig: 10

Outer Oxide Surface
Six Hours Oxidation
(700X)

Fig: 11

Outer Oxide Surface of Alloy 10
Showing Alternate NiO and Cr_2O_3 Fields
(150X)

500X

2000 X

Fig. 12

Cr_2O_3 Regions on Surface of Alloy 10 (16.5 At^{o}/o Cr)

metal with increased chromium content. The tendency of the outer layer of NiO to separate from this substrate upon cooling increased with chromium addition. A small amount of the substrate adhered to the inner surface of the large NiO crystals making it difficult to observe the structural details of this inner surface. Fig. 13 shows the only successful attempt at revealing some detail of the inner surface of the large NiO crystals. The triangular pattern, characteristic of growth on the octahedral (111) planes is clearly shown. In Fig. 14, the more typical appearance of this inner surface is shown. Undoubtedly, the bulk of this field is occupied by the substrate. A further discussion of the oxide structure is deferred to a later section.

The M^2-θ characteristics for alloys 1-6 are shown in Figs. 15 and 16. Within the limits of data interpretation, alloys 1-7 exhibited the linear relationship between M^2 and θ identified with the parabolic growth process. The oxidation rates for alloys 8, 9 and 10 were obtained by averaging the results of multiple tests with six hour exposure. Assumption of the validity of the parabolic growth law is, of course, implicit in this procedure. Gulbransen and Andrew (26) reported parabolic growth behavior at 850C for an 80 nickel-20 chromium alloy. This would appear to justify the test procedure used for alloys 8, 9 and 10, in view of the application of the parabolic law to the lower chromium alloys at the present test temperature.

The parabolic rate constants determined from the present tests are given in Table 3. The average deviation from the mean

Fig. 13

Inner Surface of Oxide of Alloy 3 After One Hour Oxidation Indicating Some Ordered Growth (700X)

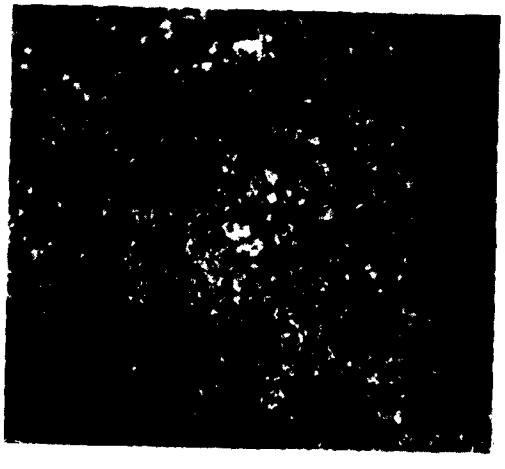

Fig. 14

Inner Surface of Oxide After One Hour Oxidation Showing Structure Typical of All Alloys (700X)

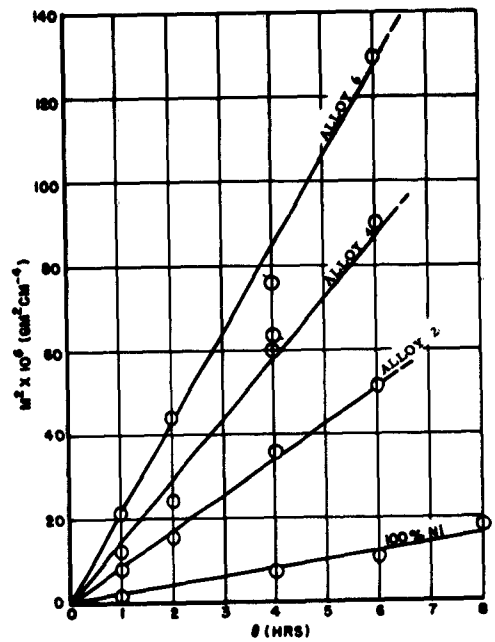

Fig: 15

M^2 - Θ Characteristic for Alloys 1, 2, 4, 6
1096°C, 76 cm Hg of O_2

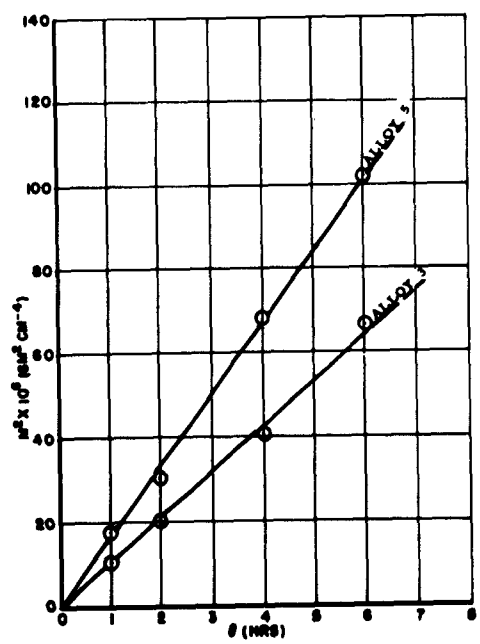

Fig: 16

M^2 - Θ Characteristic for Alloys 3, 5
1096°C, 76 cm Hg of O_2

Table 3

Oxidation Data For Nickel-Chromium Alloys

1096C
76 cm Hg of O_2

Alloy	Wgt°/o Cr	At°/o Cr	K_p ($gm^2 cm^{-4} sec^{-1}$)	K_p/K_p^o
1	0.00	0.00	5.48×10^{-10}	1.00
2	0.32	0.36	23.6×10^{-10}	4.30
3	0.92	1.04	29.7×10^{-10}	5.42
4	2.00	2.25	39.6×10^{-10}	7.22
5	3.45	3.88	46.8×10^{-10}	8.55
6	5.67	6.37	58.5×10^{-10}	10.7
7	7.64	8.55	67.8×10^{-10}	12.4
8	8.71	9.70	30.8×10^{-10}	5.63
9	11.10	12.30	3.79×10^{-10}	0.69
10	14.90	16.50	0.35×10^{-10}	0.064
	20.0	22.0	0.07×10^{-10}	0.013*

*Given in private communication to author by Dr. E. A. Gulbransen of Westinghouse Research Laboratory.

K_p values reported was about 4°/o for alloys 2-8 (incl). For the alloys exhibiting lower oxidation rates--1, 9 and 10--the average deviations from the reported values were 10, 12 and 50°/o, respectively. Obviously the data for alloy 10 are included only to show order of magnitude. The reported K_p values for all alloys were obtained by an arithmetic average of the results obtained with from four to eight specimens. Designating the parabolic rate constant for pure nickel as K^o_p, the ratio of the alloy rate constant, K_p, to that of pure nickel is given as a function of At°/o chromium in Figs. 17 and 18. In the latter figure the rate ratio is plotted on a log scale in order to make more evident the rapid decline in oxidation rate with high chromium addition. Dr. E. A. Gulbransen of the Westinghouse Research Laboratory, kindly supplied the rate data for the 22At°/o chromium alloy in a private communication to the author.

In the plot of Fig. 17 there appears to be a linear dependence of the oxidation rate on the chromium content between 0.36 and 8.6 At°/o chromium. A definite slope change is indicated at about 2At°/o chromium. The maximum oxidation rate was observed at about 8.6At°/o chromium. Time did not permit the preparation of the number of alloys required to gain a better definition of the curve in the regions of the slope change and the maximum. The log plot of Fig. 18 indicates, however, that the maximum rate is not far removed from that corresponding to 8.6At°/o chromium. With chromium addition to 9.7At°/o, the oxidation rate had decreased to about ½ of the indicated maximum rate. With 16.5At°/o chromium

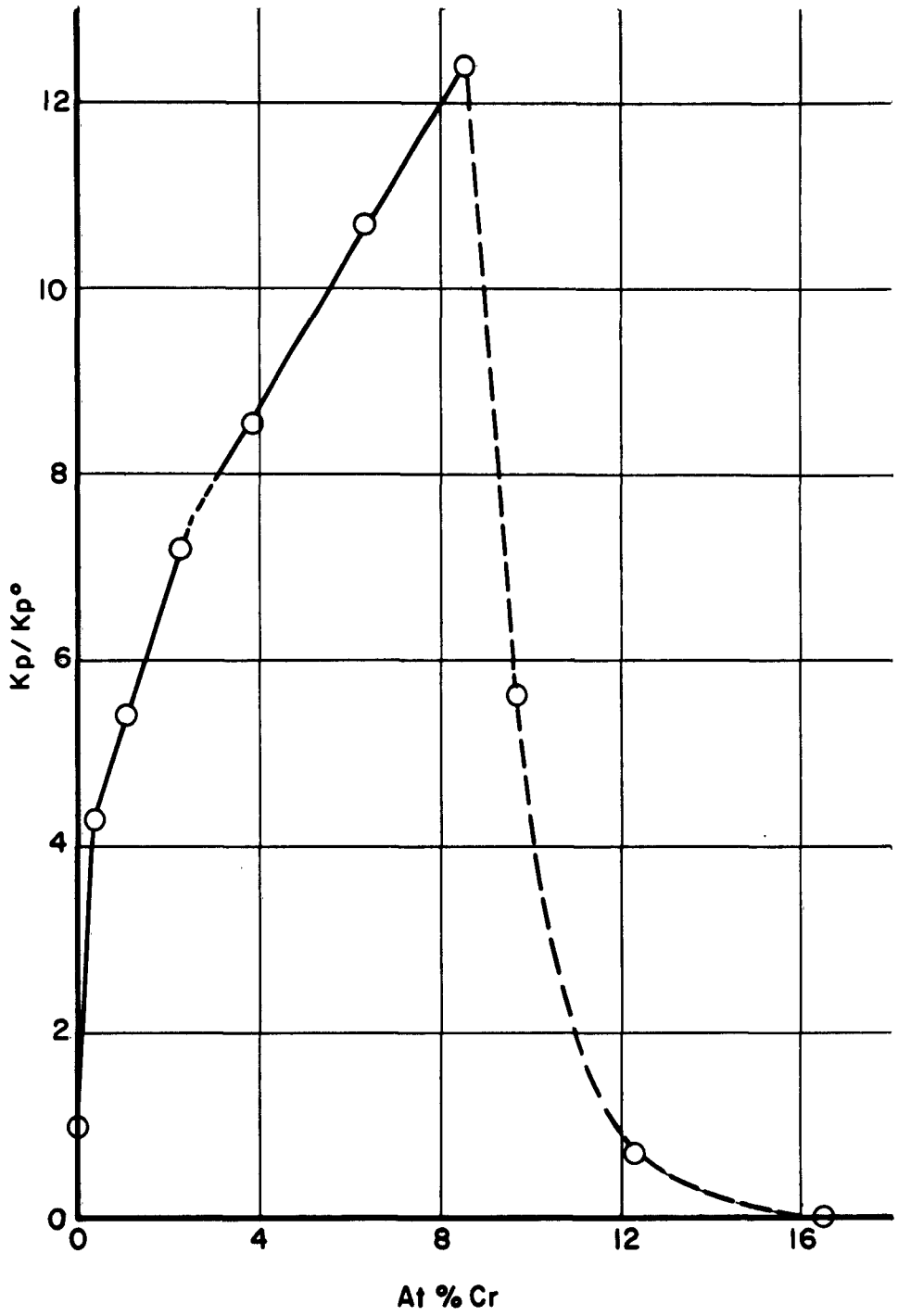

Fig: 17

K_p/K_p^o vs. At % Cr

1096°C
76 cm Hg of O_2

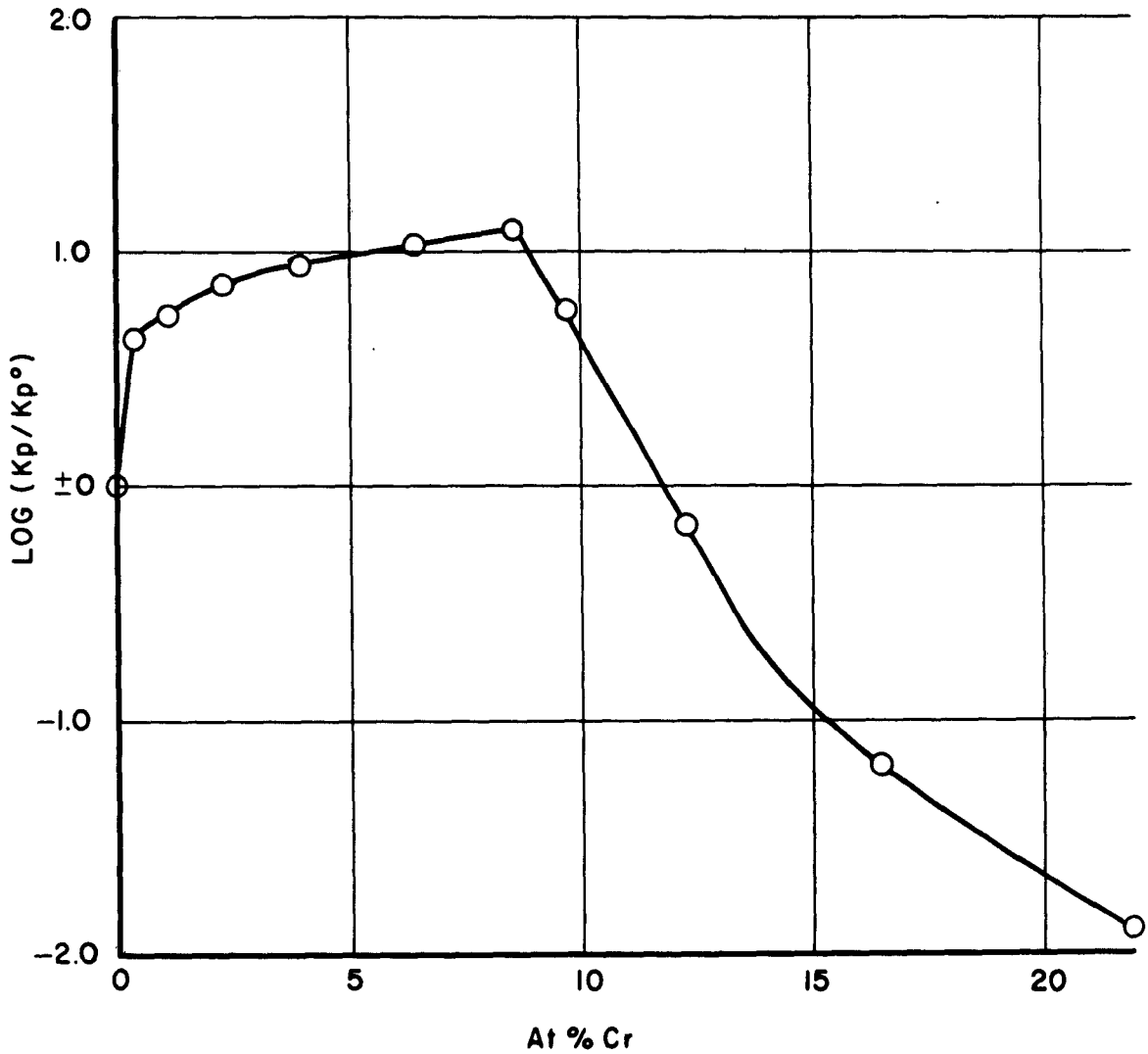

Fig: 18

$Log(K_p/K_p^o)$ vs. At °/o Cr

1096°C
76 cm Hg of O_2

the rate had decreased to about 1/200 of the maximum rate. The rapid increase in oxidation rate with the first chromium addition (0.36At°/o) is noteworthy. A significant study of this interesting low chromium region (.05 to .3At°/o) necessitates the reduction of the impurity content in the alloy to a level which appears to be difficult of attainment with the present melting techniques.

The effect of temperature on the oxidation rate-chromium content relationship is obviously important. Time did not permit the extensive additional testing required to gain these data. Wagner and Zimens (17) work on nickel-chromium alloys was conducted at 1000C. Unfortunately their alloy selection did not permit a definition of the maximum rate. Horn (16) conducted tests on nickel-chromium alloys in air at 900C. Horn's data indicate a maximum rate near 6.6At°/o chromium for this lower temperature. The data of Wagner and Zimens, and Horn, are plotted in Fig. 19 and tabulated in Table 4. Horn's data, compared with the present data, indicate that there is a shift in the oxidation maximum along the chromium axis with a 200C decrease in temperature.

D. Effects of Cold Work

Although the relation of grain size to oxidation rate has not been developed to any extent, the strong effects of grain boundaries in diffusion processes are well known and it is reasonable to expect some grain boundary influence on the oxidation rate. Siebert and Upthegrove (27) reported a small increase in the oxidation rate of mild steel at 927C with decreasing grain size. A very limited grain size study was conducted with the nickel-chromium material

Table 4

Oxidation Data for Nickel-Chromium Alloys
From Refs. 16, 17

Wgt°/o Cr	At°/o Cr	T (°C)	pO_2 (cmHg)	K_p ($gm^2 cm^{-4} sec^{-1}$)	Source
0.00	0.0	900	air	0.28×10^{-10}	Horn (16)
1.97	2.2	900	air	4.9×10^{-10}	Horn (16)
4.12	4.6	900	air	5.8×10^{-10}	Horn (16)
5.89	6.6	900	air	8.2×10^{-10}	Horn (16)
8.00	8.9	900	air	0.0×10^{-10}	Horn (16)
0.00	0.00	1000	76	3.48×10^{-10}	Wagner-Zimens (17)
0.30	0.34	1000	76	15.0×10^{-10}	Wagner-Zimens (17)
1.00	1.13	1000	76	25.8×10^{-10}	Wagner-Zimens (17)
3.00	3.38	1000	76	28.3×10^{-10}	Wagner-Zimens (17)
10.0	11.2	1000	76	5.55×10^{-10}	Wagner-Zimens (17)

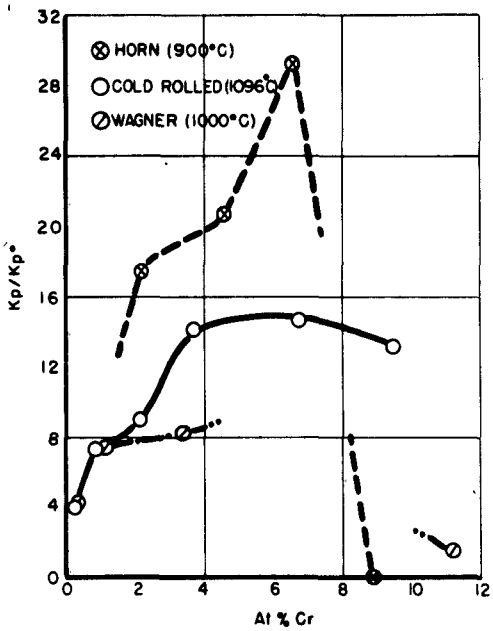

Fig: 19

K_p/K_p^o vs. At °/o Cr

For

Cold Rolled Material-1096°C, 1 Atm O_2
Horn-900°C, air
Wagner and Zimens-1000°C, 1 Atm O_2

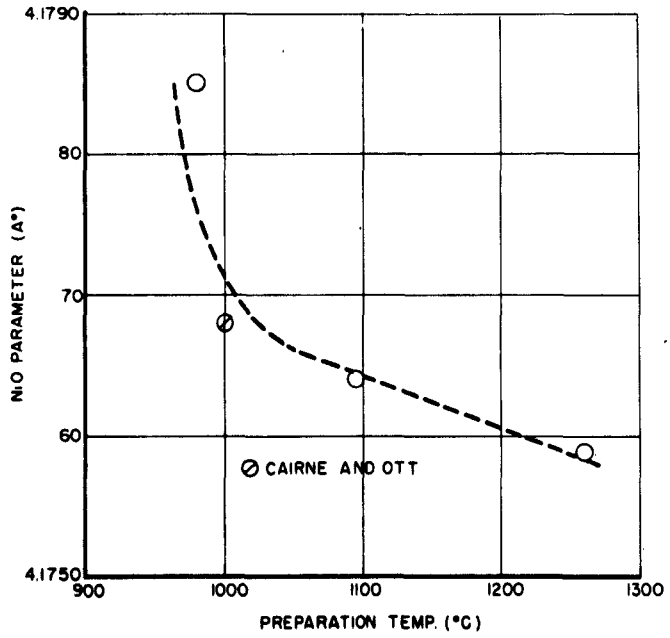

Fig: 20

NiO Lattice Parameter vs. Preparation Temperature

of the present work. Specimens of the pre-annealed alloys 1-7 were cold rolled from 0.020" to about 0.008". The unannealed material was then given the same surface treatment accorded the large grained specimens. Oxidation rate data were obtained by averaging the results of multiple six hour exposures for each alloy. These data are given in Table 5 and are plotted in Fig. 19. With the exception of alloys 1, and 2 , the cold rolled material yielded oxidation rates which were substantially higher than the rates of the corresponding large grained material. These data indicate a maximum oxidation rate at roughly 6At°/o chromium. The shape of the K_p/K_p^o-At°/o chromium relationship is markedly different from that obtained with the large-grained material. It is interesting that the maximum of the cold rolled curve is roughly at the same chromium position as the maximum of Horn's data. Horn did not specify the condition of the alloys prior to oxidation. The substantial difference between the oxidation properties of some of the cold worked material and the corresponding annealed material--persisting even with development of thick oxide films--indicate that the metal structure factor is not negligible, as has apparently been assumed by some workers. The effect of cold work on the oxidation rate is an interesting aspect of the oxidation process of great technical importance.

Table 5

Oxidation Data For Cold Worked Material

1096C
76 cm Hg of O_2

Wgt°/o Cr	At°/o Cr	K_p ($gm^2 cm^{-4} sec^{-1}$)	K_p/K_p^o
0.00	0.00	5.10×10^{-10}	1.00
0.20	0.23	21.1×10^{-10}	4.14
0.76	0.86	38.3×10^{-10}	7.50
1.87	2.11	45.9×10^{-10}	9.00
3.28	3.70	72.5×10^{-10}	14.2
6.02	6.74	74.7×10^{-10}	14.7
8.46	9.45	67.3×10^{-10}	13.2

V. PHASE AND STRUCTURE OBSERVATIONS

A. Pure NiO

Some of the evidence for establishing NiO as a metal deficit oxide has been discussed. Although a number of workers have made lattice parameter studies of NiO, the relation between the oxygen excess and the lattice parameter remains obscure. In a recent work, Brownlee and Mitchell (28) measured the parameter for several nickel oxides, prepared at different temperatures, in air, or oxygen atmospheres. Their results, compared with parameters obtained by others, notably Cairns and Ott (8), do not clarify the effect of oxygen. One difficulty appears to be the considerable variation in purity of the NiO used by various workers. Another factor, perhaps contributing to the ambiguity of reported results, is the effect of quenching from the preparation temperature. Apparently very little has been done to determine the effect of quenching rate on the retention of defects characteristic of high temperatures.

The pure nickel oxides obtained in this work at 980C, 1096C and 1260C, were analyzed with a back reflection camera, using Cu $k\alpha$ radiation ($\lambda = 1.54050$ A^{o}). Only the oxide zone which had been adjacent to the oxygen atmosphere was analyzed, primarily because of the difficulty in removing the pure NiO from the metal base. Molybdenum powder ($a = 3.14665$ A^{o}) was used to calibrate all the films. The 333 NiO line was used to determine the parameter. It was noticed that line broadening increased considerably with decreasing preparation temperature. The results of these back reflection tests, and some parameter values obtained by

other workers, are given in Table 6. If the parameters are plotted against the preparation temperature (Fig. 20), there appears to be some consistency between the present parameter data and the value reported by Cairns and Ott. Such a plot, however, implies that the oxygen excess characteristic of the preparation temperature obtains. Without better knowledge of the quenching effect, such an assumption is unjustified. It is possible that oxide parameter measurements obtained from the powdered oxides would have agreed somewhat better with the results of Brownlee and Mitchell. Subsequent parameter studies of the nickel-chromium oxides showed that the bulk parameter was slightly higher than that obtained by back reflection from the outer surface.

B. Nickel-chromium Oxides--Six Hour Development

An attempt was made to identify the phases and obtain some knowledge of the phase distribution in the oxides generated by the nickel-chromium alloys. Time limited this study to the oxides formed after six hours oxidation, at 1096C and 76 cm Hg of O_2. In an analysis of the possible oxides for the nickel-chromium-oxygen system, Gulbransen and McMillan (29) summarized many of the results of other workers and the results of their own experimental and thermodynamic studies. There are three oxides which appear to predominate as stable constituents in the nickel-chromium oxide complex, namely: NiO, Cr_2O_3, and the spinel, $NiCr_2O_4$. In the oxidation of nickel, NiO is the only oxide which has been observed. In the oxidation of nickel-chromium alloys, generally

Table 6

NiO Lattice Parameter Values From Several Sources

Temp. of Preparation (°C)	a(NiO) (A°)	Source
980	4.1785*	Present work
1000	4.1768	Cairns and Ott (8)
1096	4.1764*	Present work
1260	4.1759*	Present work
1200	4.1794	Brownlee and Mitchell (28)
1300	4.1779	Brownlee and Mitchell (28)

*back reflection value from outer (→gas) surface

with high (> 20At°/o) chromium content, various workers have reported the simultaneous existence of NiO, Cr_2O_3 and spinel, as well as combinations of two of these oxides, usually NiO and Cr_2O_3. The electron diffraction work of Hickman and Gulbransen (30), and X-ray studies of Lustman (31) on high chromium, nickel-chromium alloys, are among the studies which have established the presence of these oxides. This work has been conducted over a wide range of oxidation temperature, under constant and cyclic heating conditions. Gulbransen and McMillan (29) observed variations in the composition of the oxide formed on an 80 nickel-20 chromium alloy which were sensitive to both temperature and time of oxidation. A variable oxide composition is also manifested by deviations, with time, from the parabolic growth law, which has been observed for the nickel-chromium alloys (26). The relative effects of the spinel and Cr_2O_3 in determining oxidation resistance of the nickel-chromium alloys have not been firmly established. Scheil and Kiwit (32) and Hickman and Gulbransen (30) concluded that Cr_2O_3 is required for oxidation resistance. In the chromium region of interest to the present work, Horn (18) suggested that the spinel was responsible for the rapid decline in oxidation rate.

As a preliminary to the present X-ray work, the spinel, $NiCr_2O_4$, was prepared as follows: 1:1 mole proportions of c.p. Cr_2O_3 and NiO were thoroughly mixed and then compacted under 63,000 psi. Three pellets were made and placed together in a furnace. Sintering was done at 1200C in air for 24 hours. The

two outer pellets were discarded and a powder pattern taken of the center pellet. The X-ray showed a strong spinel pattern, with weak NiO. No Cr_2O_3 could be detected. The prepared spinel was a dark blue-green in color.

The oxides formed on all the nickel-chromium alloys, as previously noted, comprised an outer layer of massive crystals and a substrate layer of almost powdery consistency. That portion designated as the outer layer, comprised almost 100°/o of the total oxide thickness for alloy 2 and decreased to less than 40°/o of the total oxide thickness for alloy 10. Although the large crystals dominated the lay er, it was observed with increasing chromium content there was increasing fine structure away from the outer surface of this layer. Specimens of the outside layer for each oxide were given three X-ray examinations where possible: back reflection patterns were taken of the inner (→metal) and outer (→gas) surfaces and a powder pattern was obtained for the bulk layer. An 11 cm camera was used for the powder work and a back reflection camera of about 13 cm film diameter was used for the back reflection work. Cu kα-radiation, with a nickel filter, was used. All films, powder and back reflection, were calibrated using a molybdenum powder standard, as previously noted. The parameter data obtained from these tests on the outer layer are given in Table 7. It is estimated that these results are significant to better than ± 0.0005 A°. Various aspects of these data will be discussed.

Table 7

NiO Lattice Parameter Data for Outer Oxide Layer
6 Hours Oxidation

1096C
76 cm Hg of O_2

At°/o Cr (alloy)	At°/o Cr* (oxide)	Outer surface (A°)	Inner surface (A°)	Bulk (A°)
0	0	4.1764	---	4.1768
0.36	0.18	4.1770	4.1760	4.1771
1.04	0.52	4.1763	4.1752	4.1768
2.25	1.12	4.1757	4.1740	4.1761
3.88	1.92	4.1762	4.1744	4.1765
6.37	3.12	4.1767	---	4.1768
8.55	4.18	4.1771	---	4.1772
9.70	4.74	4.1764	---	4.1767
12.30	6.00	4.1760	---	4.1758
16.50	7.92	---	---	---

*Assuming $(Ni/Cr)_{alloy} = (Ni/Cr)_{oxide}$

There has been little work to establish the effect of additives on the NiO lattice parameter. The thermoelectric studies of Parravano (15), previously cited, confirmed that the addition of small amounts of chromium occurs in the way suggested by Eq. 9 of Section II. However, no lattice parameter measurements were made for the nickel-chromium mixed oxide. Brownlee and Mitchell (28) prepared a series of nickel oxides with various lithium additions, and determined the lattice parameter as a function of the lithium content. The lithium addition range was from about 0.12 to 1.0 At°/o lithium. They reported a continuous decrease in the parameter with lithium addition, the largest parameter corresponding to about 0.12At°/o lithium. Extrapolating the parameter-lithium content curve to 0°/o lithium, they obtained a value of 4.1810A°. This value was higher than values obtained for the pure nickel oxides which they prepared. This would suggest the presence of a maximum parameter between 0°/o, and 0.12At°/o lithium. Basing their argument entirely on size factors, Brownlee and Mitchell reasoned that the effect of the first small lithium additions was to fill the nickel vacancies normally existing in pure NiO. The substitution of an Li^{1+} for a nickel vacancy would cause the transition: $Ni^{3+} \rightarrow Ni^{2+}$, assuming the ionization of the lithium atoms is solely at the expense of the Ni^{3+} ions, i.e., does not involve lattice extension. The Goldschmidt radii for Ni^{3+}, Ni^{2+} and Li^{1+} are: 0.35, 0.70 and 0.78A°, respectively. Assuming the decrease in vacancies has either a negligible effect or causes a lattice expansion, then the transitions $Ni^{3+} \rightarrow Ni^{2+}$ will cause a lattice

expansion. This process will continue until the original nickel vacancies disappear. At the point of zero vacancy content, Brownlee and Mitchell argue that the lattice parameter should be a maximum, i.e., the lattice contains its maximum ratio of Ni^{2+} to Ni^{3+}, no vacancy content, and the substituted Li^{1+} ions are roughly equivalent in size to the Ni^{2+}. Proceeding with further lithium addition, the parameter should decrease due to the generation of one Ni^{3+} for each Li installed in the NiO lattice. The defect model at this point is expressed by Eq. 12, of Section II.

Reasoning similar to that employed by Brownlee and Mitchell can be applied to NiO with small chromium additions. The initial chromium additions probably have some effect on the nickel vacancy concentration obtaining with pure NiO. It might be expected that the equilibrium vacancy concentration for NiO with a small chromium content is lower than for pure NiO as long as Ni^{3+} are available to accept electrons from the added chromium. The simple defect model for the nickel-chromium mixed oxide expressed by Eq. 13 of Section II predicts a vacancy concentration equal to one half the chromium concentration. Such a model is usually applied with the preface that the concentration of defects associated with pure NiO is negligible with respect to the chromium concentration. For very low chromium concentrations, however, it is evident that the defect condition obtaining for pure NiO must be considered. It is not improbable that the effects of very small chromium additions are to reduce both the vacancy and Ni^{3+} concentrations. This implies that the original chromium ions occupy normally

vacant sites and that chromium ionization occurs partially at the expense of Ni^{3+} ions. This model is expressed by Eq. 9 of Section II. According to Eq. 4 of Section II, the initial (pure NiO) vacancy concentration is equal to one half the Ni^{3+} concentration. If it is assumed that the first chromium ions occupy the nickel vacancies associated with pure NiO, then, at the point of disappearance of the vacancies, the residual Ni^{3+} concentration will be roughly equal to the chromium concentration. The ionization of chromium atoms added to the lattice beyond this point could continue to be achieved at the expense of the Ni^{3}, causing further transitions, $Ni^{3+} \rightarrow Ni^{2+}$, according to the reaction:

$$\tfrac{1}{2}O_2 + Ni^{3+} + Cr \rightarrow O^{2-} + Cr^{3+} + Ni^{2+} \qquad (14)$$

It would seem that this process could continue, without the reappearance of nickel vacancies, until exhaustion of the original Ni^{3+}. This greatly oversimplified treatment would thus predict an <u>increase</u> in the lattice parameter with chromium addition until the Ni^{3+} originally associated with pure NiO are destroyed. With negligible Ni^{3+} concentration, the nickel-chromium mixed oxide defect model expressed by Eq. 13 of Section II could be applied. For this model, the vacancy concentration is equal to one half the chromium concentration. Assuming a parallelism between FeO, TiO (NaCl structure, metal deficit oxides) and NiO, the effect of a vacancy increase would be to <u>reduce</u> the lattice parameter. This reduction would be expected to persist until the

chromium concentration reached a saturation value with the development of a new phase. This is in contrast to the reduction observed by Brownlee and Mitchell, where the reduction was attributed to the increase in the small Ni^{3+} ions.

The trend in lattice parameter with chromium addition, postulated above, was observed for the back reflection data of the outer surface, shown in Fig. 21 out to a limit of about 2.3At°/o chromium. The data indicate a maximum parameter between 0 and 0.36At°/o chromium. The maximum, as drawn in Fig. 21, corresponds to a chromium content in the oxide of 0.18At°/o, assuming the Ni/Cr ratio in the alloy is maintained in the oxide. Obviously neither the present data, nor those of Brownlee and Mitchell, permit a good determination of the addition content corresponding to the maximum parameter. The highest parameter values were observed for the lowest additions. As a rough check on the defect models discussed above for the Ni-Li-O and Ni-Cr-O systems, it may be assumed that the maximum parameters occurred at the lowest reported lithium and chromium contents.

With lithium additions, it is assumed, with Brownlee and Mitchell, that at the composition corresponding to the maximum parameter the Li^{1+} ions have just filled the nickel vacancies associated with pure NiO. Further addition will go into an extension of the NiO lattice, with the creation of an Ni^{3+} for each Li^{1+} added. The oxygen excess in pure NiO may be defined:

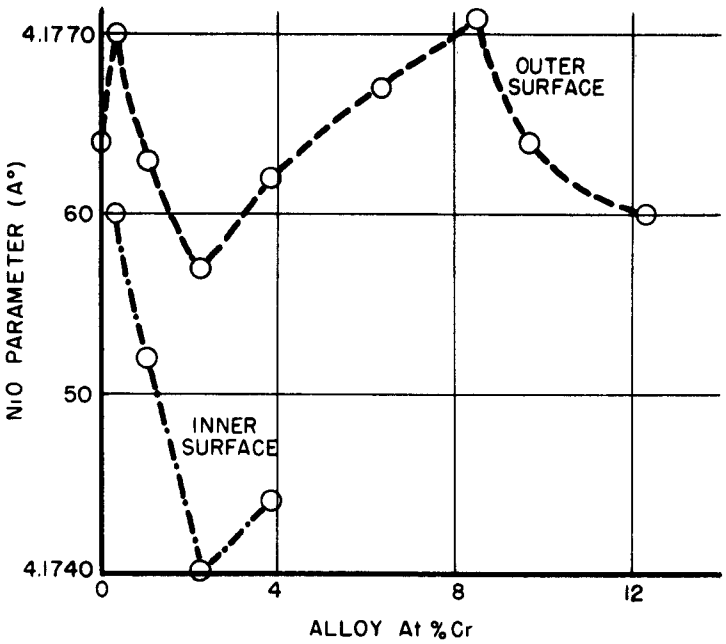

Fig: 21

NiO Lattice Parameter vs. At °/o Cr
For
Outer and Inner Surfaces of Outside Oxide Layer

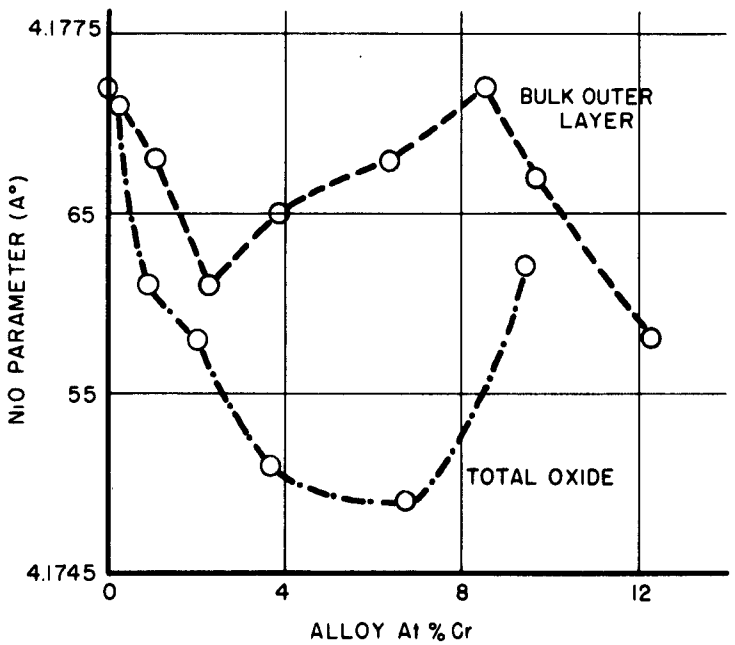

Fig: 22

NiO Lattice Parameter vs. At °/o Cr
For
Bulk Outer Layer and Total Oxide

$$At^{o}/oO_{ex} = \frac{O_{ex} x 100}{Ni + O_{stoic}} = \frac{\square Ni^{2+} x\ 100}{Ni + O_{stoic}}$$

where O_{stoic} is the oxygen associated with the nickel on a 1:1 atom basis and $\square Ni^{2+}$ is the vacancy number existing for pure NiO. Assuming the lithium occupy all the original vacancies then,

$$At^{o}/oO_{ex} = \frac{Li^{1+} x\ 100}{Ni + O_{stoic}} \backsim At^{o}/o \text{ lithium}$$

Using Brownlee and Mitchell's value of $0.12 At^{o}/o$ lithium, then

$$At^{o}/oO_{ex} \backsim 0.12$$

With chromium additions, it is assumed that the maximum parameter occurs when the Ni^{3+} have been exhausted by the chromium. If $\square Ni^{2+}$ and Ni^{3+} again refer to the defect numbers occurring in pure NiO, then at the maximum parameter point:

$$Cr^{3+} = Ni^{3+}$$

$$\therefore \quad \text{Now} \quad \square Ni^{2+} = \tfrac{1}{2} Ni^{3+}$$

$$\text{therefore,} \quad \square Ni^{2+} = \tfrac{1}{2} Cr^{3+}$$

$$\text{and } At^{o}/oO_{ex} = \frac{\square Ni^{2+} x\ 100}{Ni + O_{stoic}} \backsim \tfrac{1}{2} \frac{Cr \times 100}{Ni + O - Cr} \backsim \frac{50}{(\frac{Ni}{Cr}) + (\frac{O}{Cr}) - 1}$$

The ratios Ni/Cr and O/Cr are found from the chemical analysis of the alloy, assuming that the Ni/Cr ratio in the alloy is maintained in the oxide. For the alloy under consideration ($0.36 At^{o}/o$ chromium), the Ni/Cr and O/Cr ratios are both equal to about 278. Substituting

this value in the expression for the oxygen excess,

$$At^{o}/oO_{ex} \backsim 50/555 \backsim 0.09$$

The oxygen excess values from these two sources are in reasonable agreement. Considering that Brownlee and Mitchell prepared their oxide at 1200C and the present oxide was obtained at about 1100C, a somewhat different value of the oxygen excess might be expected for the 1200C oxide. It is interesting to compare these values with oxygen excess data reported by Baumbach and Wagner (11) and Parravano (15). Wagner prepared NiO at 1000C and by chemical analysis concluded that the oxygen excess would be $\backsim 0.002$ grm atom O/grm mole NiO. This would be equivalent to $\backsim 0.1$ At^{o}/oO_{ex}. Parravano prepared NiO at 900C. Using chemical analysis, he reported a value of $0.16 At^{o}/oO_{ex}$. These oxygen excess data for NiO are summarized in Table 8. The agreement between values of the oxygen excess obtained by chemical analysis and by lattice parameter measurements, with use of the simple defect model, is good, considering the variable preparation temperature.

For chromium contents up to about $2.3 At^{o}/o$, the lattice parameter data--particularly those of the outer surface--are in reasonable support of the defect models expressed by Eqs. 9, 13 and 14. This statement is, of course, entirely dependent on the assumption that a vacancy increase in NiO will effect a lattice contraction. Density studies, combined with chemical analysis, would be needed to test the validity of this assumption.

With alloy chromium contents greater than about $2.3 At^{o}/o$, the NiO parameter, both for the outer surface and the bulk oxide

Table 8

Summary of Some Oxygen Excess Data for NiO

Prep. Temp. (°C)	Oxygen Excess (At°/o)	Method	Source
900	0.16	chem. analysis	Parravano (15)
1000	0.10	chem. analysis	Baumbach and Wagner (11)
1096	0.09	X-ray-defect model	Present work
1200	0.12	X-ray-defect model	Brownlee and Mitchell (28)

layer, showed an unexpected behavior. Between 2.3 and 8.6At°/o chromium the parameter increased. Such a trend would suggest that new phases are competing for the chromium, with a consequent effect on the NiO vacancy content. Bulk oxide (powder) patterns of the outer layer showed traces of Cr_2O_3 and the spinel at 3.9At°/o chromium. The spinel and Cr_2O_3 patterns increased in intensity with further chromium addition (except as subsequently noted). The marked difference in appearance between the outer layer and the substrate suggested that the Cr_2O_3 and the spinel might be concentrated in the substrate region. Accordingly, three series of X-ray pictures were taken of the substrate. In the first, an attempt was made to remove as much substrate as possible without deep scribing. This material is designated as the bulk substrate. The second and third series were taken of substrate material obtained by shallow and deep scribing of the substrate layers, respectively. It was hoped that the shallow substrate material would provide information on phases predominating in the oxide just below the outer layer of massive crystals. The deep substrate tests were made to obtain some knowledge of the oxide layer contiguous to the metal-oxide interface. The granular consistency of the substrate layer made it impracticable to attempt a more quantitative depth survey. Obviously when the oxide comprising both the outer layer and the substrate was thin, the destinction between these zones was no longer significant in view of the technique used to obtain the substrate material. The line intensities of the NiO, Cr_2O_3, and the spinel, were referred to a calibrated intensity strip. The background of most of the films was too strong to permit the use of

more sensitive densitometry. For the intensity comparisons, the NiO (111), Cr_2O_3 (211) and spinel (220) lines were used. The results of this substrate analysis are given in Figs. 23, 24 and 25.

The bulk substrate data, plotted in Fig. 23, showed several features of interest. The spinel intensity appeared to reach a maximum in the neighborhood of the chromium content corresponding to the highest oxidation rate. The spinel intensity then decreased to zero somewhere between 12 and 16At°/o chromium--the region corresponding to the rapid decline in oxidation rate (of Figs. 17 and 18). The Cr_2O_3 intensity in the bulk substrate analysis showed an almost continuous increase with chromium addition, starting with the trace observed at 1.04At°/o chromium and continuing to the chromium limit of the tests. The decrease in Cr_2O_3 near 12 At°/o chromium may not be significant in view of the intensity measuring technique. However, this Cr_2O_3 decrease was noted in both the bulk and deep substrate data. In addition, the deep substrate tests showed an increase in the spinel at about 12 At°/o chromium, which may correspond with the Cr_2O_3 decrease. The deep and shallow substrate tests indicated that the spinel was concentrated near the outside NiO layer and the Cr_2O_3 near the metal. As shown in Fig. 24, the intensity ratio, spinel: Cr_2O_3, was substantially higher for the shallow layer than for the deep layer. The shallow layer data were not continued beyond 10 At°/o chromium because the very thin oxides made it impossible to obtain a satisfactory distinction between the shallow and bulk substrate material without a more refined depth control of the sampling.

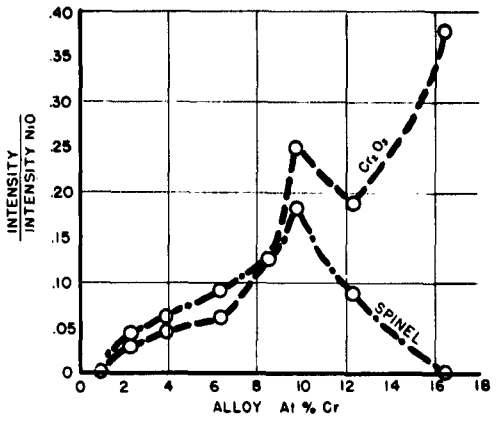

Fig: 23

Cr_2O_3 and Spinel Intensities vs. At°/o Cr
For
Bulk Substrate

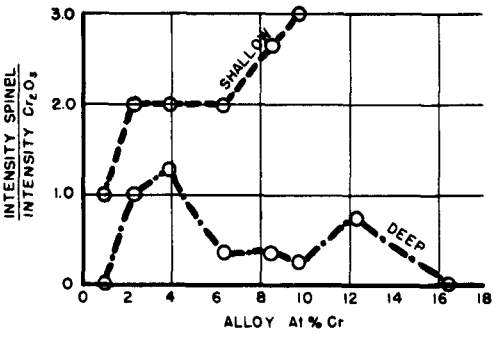

Fig: 24

Ratio of Spinel and Cr_2O_3 Intensities vs. At°/o Cr
For
Deep and Shallow Substrate

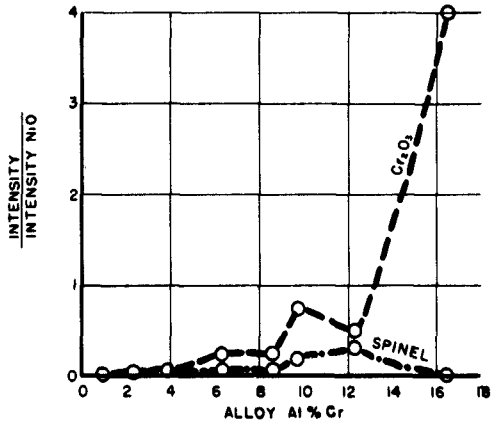

Fig: 25

Cr_2O_3 and Spinel Intensities vs. At °/o Cr
For
Deep Substrate

The increase in Cr_2O_3 with chromium addition was most evident for the deep substrate layer (Fig. 25). For the high chromium alloy, the deep substrate intensity of Cr_2O_3 relative to that of NiO, indicated the presence of an almost continuous layer of Cr_2O_3 near the oxide-metal interface.

The deep substrate diffraction patterns, in addition to showing the phase intensity variation discussed above, also showed lines which were identified with the alloy. In the process of scribing the substrate, it was impossible to avoid the removal of some of the base metal. These metal lines, however, became stronger with greater chromium addition, suggesting some coupling with the oxide formation. In an effort to fix the source of these lines, the lattice parameters of the alloys were determined. After removing the 6 hour oxide by abrasion, the alloy was filed on the surface and the filings passed through 200 mesh screen. The powder was annealed for about 10 minutes at 540C. Molybdenum powder was mixed with the alloy powder for film calibration. The results of the parameter determinations are given in Table 9 and plotted in Fig. 26. Within the data limits, the alloy parameter was found to increase linearly with chromium content. (Goldschmidt atomic radii for chromium and nickel are 1.28 and 1.25 A^o, respectively). The value obtained for the pure nickel, 3.5244 A^o, agrees fairly well with the value 3.5238 A^o, given in Barrett (33) for pure nickel. Unfortunately, the metal lines in the deep substrate pattern were very diffuse in the back reflection region, preventing a precise parameter determination. Parameter values

Table 9

Lattice Parameter Data For Nickel-Chromium Alloys
and for
Metal Constituent in Oxide

Wgt°/o Cr	At°/o Cr	a(alloy) (A°)	a(metal constituent in oxide) (A°)
0.00	0.00	3.5244	---
3.45	3.88	3.5277	---
5.67	6.37	3.5306	---
7.64	8.55	3.5317	3.5260
8.71	9.70	---	3.5249
11.10	12.30	3.5352	3.5283
14.90	16.50	3.5407	3.5261
			$\bar{a}$: 3.5263

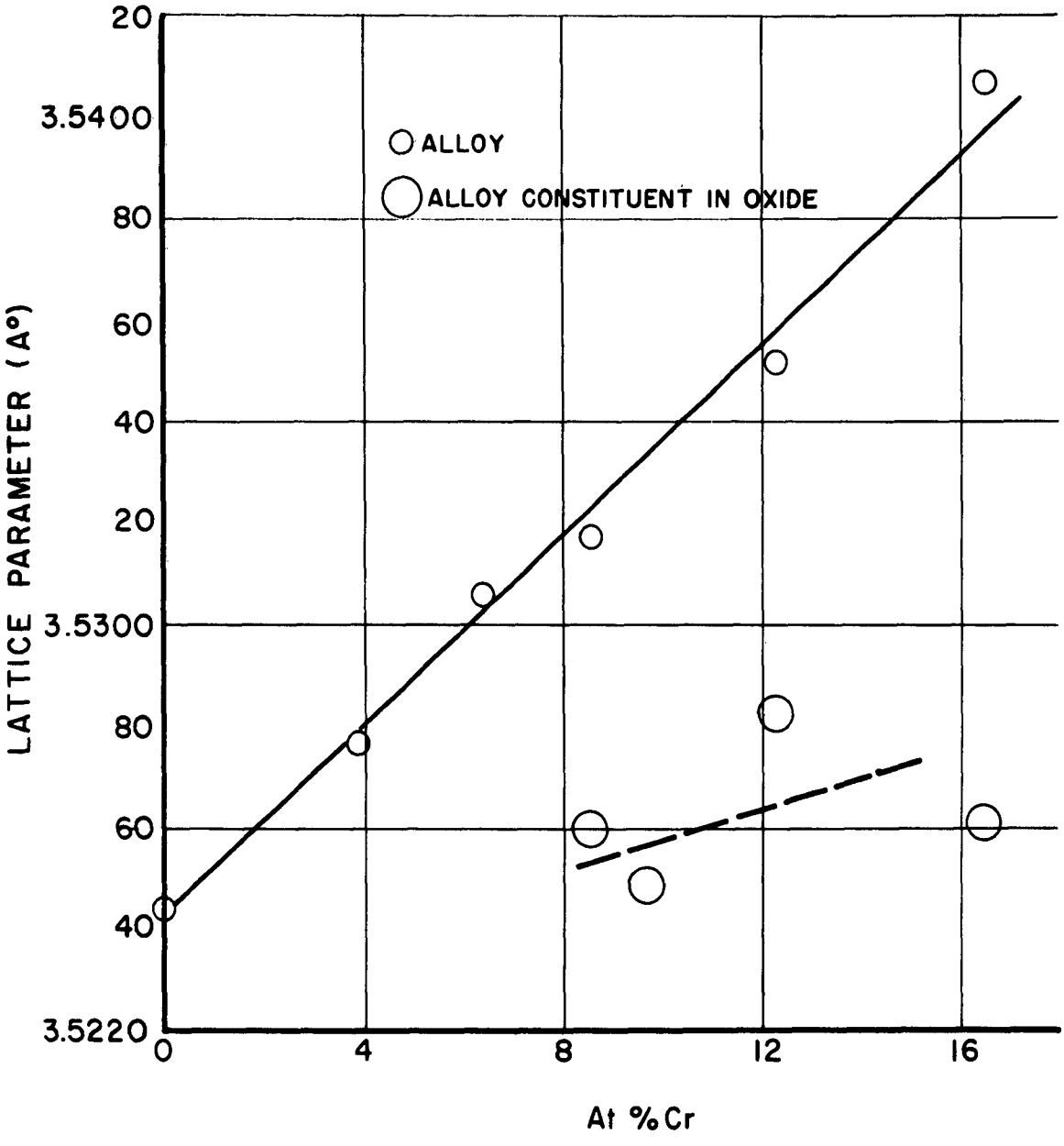

Fig: 26

Ni-Cr Alloy Lattice Parameter vs. At % Cr

were obtained by an average of the front reflection data, using molybdenum powder to calibrate the film in this region. In spite of the considerable scatter in the latter data, it is evident from Fig. 26 that the metal lines in the oxide could be derived from two sources: alloy with strong chromium depletion, or pure nickel. The possibility of pure nickel is interesting in that it would help confirm the solid state displacement reaction,

$$2\,Cr + 3\,NiO \longrightarrow Cr_2O_3 + 3Ni \qquad (15)$$

given by Gulbransen and McMillan (29) as a possible mode of generation of Cr_2O_3 within the oxide. The arithmetic average of the parameters found for the metal constituent in the oxide was 3.5263 A^o, which does not exclude the possibility that these lines are attributable to nickel, considering the scatter in the data. The fact that the metal lines increased in intensity with increasing Cr_2O_3 intensity may be additional support for the above reaction.

It was observed previously that the oxidation rate-chromium content relationship showed a transition near 2 At^o/o chromium (cf Fig. 17). Considering that the parabolic type of oxide growth is diffusion controlled, this transition to a somewhat lower slope $\frac{d(K_p/K_p^o)}{d(At^o/o\ Cr)}$ would suggest the appearance of new phases, or a change in the defect structure of the NiO. As it is somewhat difficult to visualize a marked change in the rate of defect generation with chromium addition, without the appearance of a competing phase, it is probable that these changes occur simultaneously. The substrate X-ray analysis showed traces of Cr_2O_3 and spinel

at the surprisingly low chromium content of 1.0At°/o. At 2.3 At°/o chromium, the spinel and Cr_2O_3 phases were apparently well established. These observations appear to support the existence of a true transition in the K_p-At°/o chromium relationship in the vicinity of 2 At°/o chromium effected by the appearance of Cr_2O_3 and spinel phases.

The lattice parameter of the outer NiO layer was found to be a minimum near 2 At°/o chromium. The change in the parameter near 2 At°/o chromium could be correlated with the appearance of the Cr_2O_3 and spinel phases. The increasing parameter with chromium addition suggests that decreasing amounts of chromium were installed in the NiO lattice, with a reduction in the vacancy content. If this view is accepted, then the minimum parameter point would correspond to the chromium saturation concentration in the NiO lattice, for the six hour oxide at least. This minimum point is equivalent to 1.1 At°/o chromium in the oxide, assuming the alloy nickel-chromium ratio is maintained in the oxide. It is interesting to note that Hauffe (34) suggests a chromium saturation of about 1.0 At°/o on the basis of conductivity tests on NiO with Cr_2O_3 additions. Hauffe observed that the conductivity decreased sharply with chromium addition and appeared to attain a constant value at roughly 0.5 mole°/o Cr_2O_3 (1.0At°/o chromium). The sparsity of Hauffe's data, however, does not permit a good determination of the chromium content where constant conductivity is established. However, on the basis of the nickel-chromium mixed oxide defect models previously discussed, the chromium

saturation point would not correspond to the point of minimum conductivity. The electrical conductivity in NiO is attributed to the presence of Ni^{3+}. On the basis of the model expressed by Eq. 13 of Section II, chromium additions to the NiO lattice would be expected to continue after the disappearance of the Ni^{3+}.

As shown in Fig. 21, the parameter data obtained by back reflection from the inner (→metal) surface of the outer oxide layer were generally lower than the corresponding data for the outside (→gas) surface. A minimum is indicated for both sets of data at about 2At°/o chromium. Again assuming the correspondence between the parameter and vacancy content, these data would indicate a substantial vacancy gradient directed toward the oxide-gas interface. This would mean diffusion in the direction of the vacancy gradient if it is assumed that the mass flow in the oxide is metal to gas. The inner surface data were not continued beyond 4At°/o chromium because the diffraction lines became exceedingly diffuse with greater chromium addition. This could indicate increasing inner surface irregularity, caused by increasing penetration of new phases into the outer NiO layer.

C. Nickel-Chromium Total Oxides

Time did not permit an extension of the six hour oxide study to other oxidation times. In an attempt to obtain a somewhat magnified picture of the oxide structure, thin (.002 →.004") specimens of the alloys containing up to 8.5 At°/o chromium were oxidized to completion under the test conditions (1096C, 76 cm Hg of O_2). These total oxidation specimens were prepared from the unannealed alloy stock. To insure complete oxidation, oxidation times

ranged from 24 to 48 hours, the former time applying to the high chromium alloy and the latter time to the pure nickel. Attempts at securing oxide cross sections of satisfactory detail with the usual sectioning and polishing techniques were not successful. The fracture technique, used by Jappfe (35), was applied to the total oxides in an effort to reveal some change in the oxide structure with chromium addition. These sections are shown in Figs. 27, 28, 29. Comparing the pure nickel section with that of alloy 7, the development of an extensive interior region of fine structure is readily apparent. This interior structure had the same appearance as the substrate previously discussed in connection with the six hour oxides. With 0.23 At°/o chromium, there appears to be some delineation of an interior zone. It is curious that the interior of this 0.23 At°/o oxide showed more change from the massive NiO crystals, characteristic of the pure NiO, than did the 0.86 and 2.1 At°/o chromium oxides. This tendency for a fine structure in the interior was noted for a number of fracture sections taken of the 0.23 At°/o oxide, and, therefore, is not peculiar to the section shown in Fig. 27. The development of a sharp boundary between the large surface crystals and the interior crystals is evident for the 0.86 and 2.1 At°/o chromium oxides. The first traces of Cr_2O_3 and spinel were noted for the six hour oxides near 1 At°/o chromium and these phases were apparently well established by 2 At°/o chromium. In the total oxide sections, no significant change in the large crystal structure is evident, even at 2.1 At°/o chromium. An interesting

100°/o Ni

Alloy 2(0.23 At°/o Cr)

Alloy 3(0.86 At°/o Cr)

Fig. 27

Fracture Sections for Total Oxides of Alloys 1, 2 and 3 (500X)

Alloy 4(2.1 At°/o Cr)

Alloy 5(3.7 At°/o Cr)

Alloy 6(6.74 At°/o Cr)

Fig. 28

Fracture Sections for Total Oxides of Alloys 4, 5 and 6
(500X)

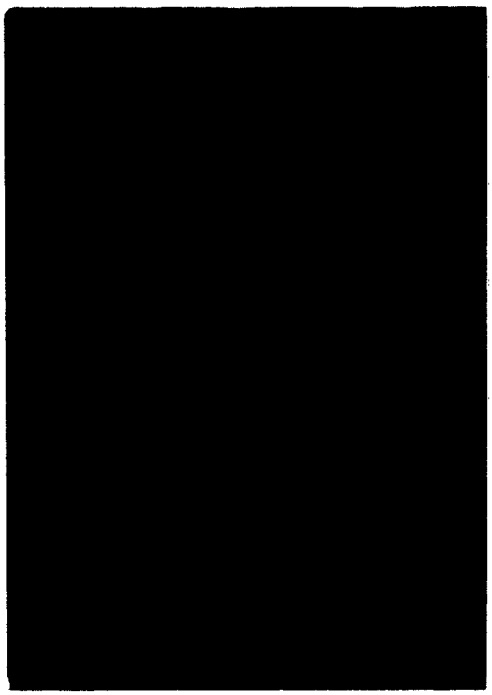

Fig: 29

Fracture Section for Total Oxide of Alloy 7 (9.45 At°/o Cr)

(300X)

Fig: 30

Outer NiO Layer of Total Oxide (Alloy 7)
Showing Some Fine Structure Development
(1000X)

banding of the oxide is evident, however, for the 2.1 At°/o chromium oxide. This banding persisted in all the oxide sections of greater chromium content. The progressive development of an interior fine structure is evident for the higher chromium oxides. The separation of the outside layer of large NiO crystals from the interior zone was very noticeable for the 9.5 At°/o oxide. It proved, in fact, to be quite difficult to obtain a full section of this oxide. In view of the X-ray analysis previously discussed, the region of fine structure must be associated with the Cr_2O_3 and spinel phases. It was not possible to differentiate between the NiO, Cr_2O_3 and spinel phases in this interior region with visual examination. For the 6.7 and 9.5 At°/o chromium total oxides an examination of the large outside crystals, at high magnification, showed what was apparently the start of fine structure development in the large crystals. This was most evident for the 9.5 At°/o oxide. A typical section, showing some fine structure development in the large crystals is shown in Fig. 30.

NiO lattice parameters were obtained for the powdered total oxides. Line widths for the total oxide patterns were comparable to those observed for the six hour bulk outer layer patterns. These results are plotted in Fig. 22 and given in Table 10. The total oxide parameter decreased with chromium addition to about 7 At°/o chromium. This corresponds to about 4 At°/o chromium in the oxide. Using the defect model previously applied to the six hour oxides, these data would indicate chromium saturation in the NiO of about 4 At°/o. The substantial difference

Table 10

Lattice Parameter Data for NiO of Total Oxides

1096 C
76 cm Hg of O_2

At°/o Cr (alloy)	At°/o Cr (oxide)	a(NiO) (A°)
0.00	0.00	4.1771
0.23	0.11	4.1771
0.86	0.43	4.1761
2.11	1.05	4.1758
3.70	1.83	4.1751
6.74	3.32	4.1749
9.45	4.18	4.1762

between this apparent saturation value and that obtained from the six hour oxide data, ($\backsim$ 1 At^{o}/o) would indicate that the six hour oxide is far removed from the equilibrium structure. In Fig. 22 it is evident that, out to the limit of the tests, the parameters for the total oxide are generally lower than the parameters of the corresponding six hour bulk oxides. This fact, and the substantial shift in minimum parameter to higher chromium content for the total oxides, suggest that much greater solution of chromium in the NiO phase has been effected by increased oxidation time. The indications of new phase development in the outer layer of the high chromium total oxides would suggest that even the 24 hour exposure was not sufficient to establish an equilibrium structure for the total oxides.

For the total oxides, it is to be noted that the decrease in parameter with chromium addition persists out to roughly the chromium content corresponding to the maximum oxidation rate, i.e., the maximum vacancy content and maximum oxidation rate are roughly coincident on the chromium axis. Had this trend been observed for the six hour oxides, the defect model could be applied to an explanation of the observed oxidation rates with greater confidence. The observations on the six hour oxides would indicate that non-equilibrium, transition, structures are controlling during the important first stages of the oxidation process. Until the defect model can be made to include these transition structures, it obviously has a somewhat limited utility.

VI. SUMMARY

The relationship of the oxidation rate to the alloy chromium content has been defined in some detail for an oxidation environment of 1096C and 76 cm Hg of oxygen. There are three parts of this relationship which are, perhaps, of equal interest from the standpoint of the oxidation mechanism. First, the large increase in oxidation rate effected by small chromium additions is of interest. With a chromium content of 0.36At°/o, the parabolic rate constant had increased by a factor of 4 over that of pure nickel. Arbitrarily designating 0.36At°/o chromium as the terminus of this first section of the K_p/K_p^o-At°/o chromium plot, the average slope of this section is:

$$\frac{d(K_p/K_p^o)}{d(\text{At}^o/o\ \text{Cr})} = 4.3/0.36 \backsim +12 \qquad \text{for } 0\text{-}0.36\text{At}^o/o\ \text{Cr}$$

Accepting the concept that the diffusion rate of nickel and chromium ions is increased by the chromium created vacancies, then a lattice contraction in the NiO should be observed, if the only effect of the chromium addition were to augment the vacancy content of the pure NiO. The Goldschmidt radii for Cr^{3+} and Ni^{2+} are 0.64 and 0.70A°, respectively. Hence, a Cr^{3+} for Ni^{2+} substitution would not be expected to increase the lattice parameter even assuming a change in the vacancy content had a negligible effect on the parameter. The lattice parameter measurements of the present work, admittedly very sparse in the low chromium region, do not show a lattice contraction, but rather an expansion with the first chromium addition. This would suggest one of the following reactions:

$$Cr + \square Ni^{2+} + 3Ni^{3+} \rightarrow Cr^{3+} + 3Ni^{2+} \qquad (16)$$

According to Eq. 16 chromium is added without lattice extension and with the destruction of 1 $\square Ni^{2+}$ and $3Ni^{3+}$ for each chromium.

$$\tfrac{1}{2}O_2 + \square Ni^{2+} + Ni^{3+} + Cr \rightarrow O^{2-} + Cr^{3+} + Ni^{2+} \qquad (9)$$

(cf Section II)

This reaction involves chromium addition with lattice extension and the destruction of 1 $\square Ni^{2+}$ and $1Ni^{3+}$ for each chromium ion.

$$\tfrac{1}{2}O_2 + Ni^{3+} + Cr \rightarrow O^{2-} + Cr^{3+} + Ni^{2+} \qquad (14)$$

(cf Section V)

This reaction implies that either the chromium ions do not occupy available vacant sites, or that previous chromium additions have filled the vacancies (possibly according to Eq. 9) and subsequent chromium addition does not create new vacancies. Reaction (14) might be expected to continue until exhaustion of the Ni^{3+}. Eqs. 9 and 14 were employed in the oxygen excess calculation of Section V.

Chromium addition according to Eq. 16 might be expected to cause the greatest increase of parameter. However, it was previously noted that Parravano (15), using a thermoelectric technique, had established a 1:1 correspondence between the chromium ions added and the Ni^{3+} destroyed. The chromium content in the nickel-chromium mixed oxide used by Parravano was about 0.5At°/o. This corresponds to about 1.0At°/o chromium in the alloy, assuming the nickel-chromium ratio in the alloy is maintained in the oxide. In Fig. 21 (cf also Table 7), it is obvious that the parameter value for the outer layer could continue to increase beyond that value

given for 0.36At°/o chromium. In Section V it was suggested that the maximum parameter might correspond to the disappearance of the Ni^{3+} in the nickel-chromium mixed oxide. Parravano's data, indicating the presence of Ni^{3+} near 1At°/o chromium (alloy) are not inconsistent with the present parameter data, considering possible differences between the oxide used in Parravano's work and the oxide of this work. Up to a chromium content of between 0.36 and 1.0At°/o, there seems to be fair support for chromium addition according to Eqs. 9 and 14. One obvious objection to the use of Eqs. 9 and 14, however, is that the initial chromium addition does not involve the creation of new vacancies. This is not consistent with the demand for a vacancy increase in explanation of the observed large increase in oxidation rate, relative to pure nickel. The present data in the low chromium region, however, are not sufficient to justify a serious challenge to the accepted defect model and the cationic vacancy diffusion mechanism.

The second part of the K_p/K_p^o-At°/o chromium relationship of interest is that between 0.36At°/o chromium and the maximum at about 8.6At°/o chromium. Within this range of chromium content, a reduction was observed in the initial high rate of increase of K_p with chromium addition. Between 0.36 and about 2.3At°/o chromium, a straight line has been fitted to the data, with a slope:

$$\frac{d(K_p/K_p^o)}{d(\text{At°/o Cr})} = \frac{2.7}{1.6} \backsim +1.7 \qquad \text{for } 0.36 \rightarrow 2.3 \text{At°/o Cr}$$

and between 2.3 and 8.6At°/o chromium, another straight line with a slope:

$$\frac{d(K_p/K_p^o)}{d(At^o/o\ Cr)} = \frac{4.6}{6.6} \backsim +0.7 \qquad \text{for } 2.3 \rightarrow 8.6 At^o/oCr$$

The X-ray analysis of the outer oxide layer showed a decrease in the lattice parameter with chromium addition between 0.36 and about 2.3At°/o chromium. This finding is in accord with the expectation of a vacancy increase with chromium addition (according to Eq. 13 of Section II). However, between 2.3 and 8.6At°/o chromium the NiO parameter increased. It is apparent from a consideration of the slopes of the above lines that a change in the effect of chromium on the oxidation rate has started at roughly 2.3At°/o chromium. The slope change, in addition to the new trend in parameter, suggests the appearance of new phases in the oxide. This was confirmed by the X-ray analysis of the oxide--particularly the substrate intensity study. Both Cr_2O_3 and the spinel appeared at about 2.0At°/o chromium. These phases increased with further chromium addition, with a concomitant increase in the oxidation rate. Apparently, there have been no previous suggestions that the diffusion rates through Cr_2O_3 and the spinel are even comparable to the rate through NiO. On the contrary, the presence of one, or both, of these phases is deemed requisite for oxidation resistance. The observation that the spinel and Cr_2O_3 are concentrated in the substrate region, together with the phase intensity data, indicates that the diffusion path must involve considerable Cr_2O_3 and spinel--particularly for the oxide corresponding to the maximum oxidation rate. Diffusion data

for Cr_2O_3 and the spinel are almost entirely lacking. However, the work of Gulbransen and Hickman, and Scheil and Kiwit, indicated that high oxidation resistance correlated with high Cr_2O_3 content in the oxide. The present X-ray data substantiate this, in that only Cr_2O_3 and NiO were in evidence in the oxide corresponding to the lowest oxidation rate. Accepting the belief that Cr_2O_3 is a barrier to the ionic current, it is then hard to reconcile the maximum oxidation rate with the high spinel content of the corresponding oxide if high diffusion resistance is assigned to the spinel as well. The dimensions of the spinel and Cr_2O_3 phases in the principal diffusion direction, as well as the distribution of these phases with respect to NiO, are additional important considerations. The present knowledge of these factors is extremely limited.

As noted above, the lattice parameter data for the outer layer of the six hour oxide showed an increase, persisting at least to the chromium content corresponding to the maximum oxidation rate. The correspondence of a maximum parameter with a maximum oxidation rate is disturbing with respect to a confirmation of the defect model (expressed by Eq. 13 of Section II) and the cationic vacancy diffusion mechanism. The present knowledge of the effect of additives on NiO does not exclude the possibility that the interstitial diffusion mechanism becomes effective over some range of the chromium concentration. The increasing NiO parameter with chromium contents in excess of about 2.3At^{o}/o could be attributed to some interstitial solution of one or more of the ions. An increasing oxidation rate could be reconciled with the increasing lattice parameter if it is assumed

that the interstitial diffusion mechanism becomes increasingly operative with chromium contents in excess of about 2.3At°/o. It is conceivable that the change in the rate of increase of K_p with chromium addition, observed near 2.3At°/o chromium, is a manifestation of the start of some interstitial diffusion in the NiO layer.

The third part of the K_p-At°/o chromium relationship of interest is that between the maximum at 8.6At°/o chromium and a point at roughly 10At°/o chromium. The slope in this region:

$$\frac{d(K_p/K_p^o)}{d(At^o/o\ Cr)} \backsim -6 \qquad 8.6 \rightarrow 10 At^o/o\ Cr$$

is indicative of a remarkable change in some property, or properties, of the oxide over a very narrow chromium range. The six hour oxide parameter data did not provide a clue. The decrease in parameter observed with chromium additions greater than about 8.6At°/o is contrary, in fact, to the association of high oxidation resistance with low vacancy concentration. The only evidence is the deep substrate intensity study which showed a rapid increase in Cr_2O_3 with chromium addition in the region of the lowest oxidation rate. From these observations, it would appear that the limit of coexistence of the spinel with NiO and Cr_2O_3 is between 12 and 16At°/o chromium (alloy) - for the six hour oxides of the present study.

The use of techniques such as micro-X-ray probing, perhaps in combination with paramagnetic resonance and dielectric studies, to gain a more detailed knowledge of the oxide structure, is certainly

indicated before a significant advance from the present theoretical position can be accomplished. The still very limited knowledge of such basic factors as the phases controlling the oxidation would seem to seriously restrict any attempts to apply mathematical models in description of the process under consideration.

VII. CONCLUSION

The present work has indicated that the simple nickel-chromium mixed oxide defect model has a somewhat limited utility when applied to the oxidation of nickel-chromium alloys. Beginning at the surprisingly low chromium content of about 2.0At°/o (alloy), there is apparently a complex exchange of chromium among three phases in the oxide- NiO, Cr_2O_3 and the spinel ($NiCr_2O_4$). This exchange was reflected in the NiO lattice parameter data and in the rate of increase of oxidation rate with chromium addition.

The X-ray data failed to correlate high mean vacancy concentration with high oxidation rate. This does not support the concept that the vacancy diffusion mechanism is primarily responsible for the oxide growth over the entire chromium range of this study. The lattice expansion observed with chromium contents greater than about 2.0At°/o, could indicate some interstitial solution of one or more of the ions involved in the oxide formation. The possibility of an interstitial diffusion being controlling over some part of the chromium range, cannot be excluded. The present observations may be seriously distorted by quenching effects. However, in some studies, such as the TiO work previously cited (19), good retention of the high temperature defect structure has been achieved with the use of quenches apparently no more severe than employed in the present work.

X-ray analysis of the six hour oxides showed a surprising congruence between the spinel intensity and the oxidation rate. If it is assumed that the coupling between X-ray intensity and concentration permits a rough interpretation of the intensity curves

in terms of concentration, then the present intensity data suggest that the spinel phase presents less resistance to diffusion than has been suspected. The rapid increase in Cr_2O_3 intensity in the chromium region corresponding to the steep decline in oxidation rate, is additional support for the belief that Cr_2O_3, rather than the spinel, imparts oxidation stability to nickel-chromium alloys.

16. Horn, L., Uber den Einfluss von Zutsatzen auf Oxydation von Nickel und Chrom-Nickel Legierungen; Z. Metallk., (1949) 40, p. 73

17. Wagner, C. and Zimens, K. E., Die Oxydationgeschwindigkeit von Nickel bie kleinen Zusatzen von Chrom und Mangan; Acta Chemica Scandinavica, (1947) 1, p. 547

18. Jette, E. R. and Foote, F., An X-Ray Study of the Wustite (FeO) Solid Solutions; J. Chem. Phys., (1933) 1, p. 29

19. Bumps, E. S., Kessler, H. D. and Hansen, M., The Titanium-Oxygen System; Trans. Amer. Soc. Met., (1953) 45, p. 1008

20. Gensch, C. and Hauffe, K., Uber die Oxydationgeschwindigkeit von Zinklegierungen; Z. Phys. Chem., (1950) 196, p. 427

21. Gulbransen, E. A., Thin Oxide Films on Iron; Trans. Electrochem. Soc., (1942) 81, p. 327

22. Gulbransen, E. A. and Andrew, K. F., The Kinetics of Oxidation of High Purity Nickel; Journal of Electrochem. Soc. (1954) 101, p. 128

23. Uhlig, H. H. and Brenner, A. E., Effects of Electric Field on Oxidation of Copper; Acta Metallurgica, (1955) 3, p. 108

24. Moore, W. J. and Lee, J. K., Oxidation Kinetics of Nickel and Cobalt; J. Chem. Phys., (1951) 19, p. 255

25. Le Blanc, M. and Sachse, H., Uber Schwarzes Nickeloxyd; Z. Electrochem., (1926) 32, p. 204

26. Gulbransen, E. A. and Andrew, K. F., Rate of Oxidation of Three Nickel-Chromium Heater Alloys Between 500 C and 900 C; J. Electrochem. Soc., (1954) 101, p. 163

27. Siebert, C. A. and Upthegrove, C., The Effect of Grain Size on the Oxidation of a Low Carbon Steel; Trans. Amer. Soc. Met., (1938) 26, p. 1051.

28. Brownlee, L. D. and Mitchell, E. W., On the Variations of Lattice Parameter of Some Semiconducting Oxides; Proc. Phys. Soc., (1952) B 65, p. 710

29. Gulbransen, E. A., and McMillan, W. R., Oxide Films on Nickel-Chromium Alloys; Ind. and Eng. Chem., (1953) 45, p. 1734

30. Hickman, J. W. and Gulbransen, E. A., An Electron Diffraction Study of Oxide Films Found on Nickel-Chromium Alloys; Trans. A.I.M.M.E., (1949) 180, p. 519

31. Lustman, B., The Intermittent Oxidation of Some Nickel-Chromium Base Alloys; Trans. A.I.M.M.E., (1950) 188, p. 995

32. Scheil, E. and Kiwit, K., Arch. Eisenhuttenw. (1935-36) 9, p. 405

33. Barrett, C. S., Structure of Metals; McGraw Hill, New York, (1943)

34. Hauffe, K., Fehlordnungsercheinungen und Platzwechselvorgange in electronenleitenden Mischphasen; Ann. Phys., (1950) 8, p. 201

35. Zapffe, C. A. and Clogg, M., Fractography--A New Tool for Metallurgical Research; Trans. Amer. Soc. for Met., (1945) 34, p. 71

DISTRIBUTION LIST

Copy Number	
1 - 2	Chief of Naval Research Department of the Navy Washington 25, D.C. Attn: Code 423
3 -8	Director Naval Research Laboratory Washington 25, D.C. Attn: Tech. Information Officer
9	Commanding Officer Office of Naval Research Branch Office 346 Broadway New York 13, New York
10	Commanding Officer Office of Naval Research Branch Office 844 North Rush Street Chicago 11, Illinois
11	Commanding Officer Office of Naval Research Branch Office 801 Donahue Street San Francisco 24, California
12	Commanding Officer Office of Naval Research Branch Office 1030 East Green Street Pasadena 1, California
13	Assistant Naval Attache for Research London, England U. S. Navy FPO No. 100 New York, New York

14 Director
Naval Research Laboratory
Washington 25, D.C.
Attn: Code 3500, Metallurgy Div.

15 Director
Naval Research Laboratory
Washington 25, D.C.
Attn: Code 2020, Tech. Library

16 - 18 Bureau of Aeronautics
Department of the Navy
Washington 25, D.C.
Attn: N. E. Promisel, AE-41

19 Bureau of Aeronautics
Department of the Navy
Washington 25, D.C.
Attn: Technical Library, TD-41

20 Commanding Officer
Naval Air Materiel Center
Naval Base Station
Philadelphia, Pennsylvania
Attn: Aeronautical Materials Lab.

21 - 23 Bureau of Ordnance
Department of the Navy
Washington 25, D.C.
Attn: Rex

24 Bureau of Ordnance
Department of the Navy
Washington 25, D.C.
Attn: Technical Library, Ad3

25 Superintendent
Naval Gun Factory
Washington 20, D.C.
Attn: Metallurgical Lab., IN910

26 Commanding Officer
U. S. Naval Ordnance Laboratory
White Oaks, Maryland

27 Commanding Officer
U. S. Naval Ordnance Test Station
Inyokern, California

28 - 30 Bureau of Ships
Department of the Navy
Washington 25, D.C.
Attn: Code 343

31 Bureau of Ships
Department of the Navy
Washington 25, D.C.
Attn: Code 337L, Tech. Library

32 U. S. Naval Engineering Experiment Station
Annapolis, Maryland
Attn: Metals Laboratory

33 Director, Materials Laboratory
Building 291, Brooklyn 1, New York
New York Naval Shipyard, Attn: Code 907

34 Bureau of Yards and Docks
Department of the Navy
Washington 25, D.C.
Attn: Research and Standards Div.

35 U. S. Naval Post Graduate School
Monterey, California
Attn: Dept. of Metallurgy

36 Chief of Staff, U. S. Army
The Pentagon
Washington 25, D.C.
Attn: Director of Research and Development

37 - 38 Office of the Chief of Ordnance
Department of the Army
Pentagon
Washington 25, D.C.
Attn: ORDTB - E. L. Hollady

39 Commanding Officer
Watertown Arsenal
Watertown, Massachusetts
Attn: Laboratory Division

40 Office of the Chief of Engineers
Department of the Army
Washington 25, D. C.
Attn: Research and Development Branch

41 U. S. Air Forces
Research and Development Division
The Pentagon
Washington 25, D. C.

42 - 43 Air Materiel Command
Wright-Patterson Air Force Base
Dayton, Ohio
Attn: Materials Laboratory - MCREXM

44 Atomic Energy Commission
Division of Research
Metallurgical Branch
Washington 25, D. C.

45 National Bureau of Standards
Washington 25, D.C.
Attn: Physical Metallurgy Div.

46 National Advisory Committee for Aeronautics
1512 H Street, N.W.
Washington 25, D.C.

47 Research and Development Board
Committee on Basic Physical Sciences
The Pentagon
Washington 25, D.C.
Attn: Metallurgy Panel

48 R. F. Mehl
Metallurgical Advisory Board
DuPont Building
Washington, D.C.

49 J. E. Dorn
University of California
Berkeley, California

50 R. J. Jaffee
Battelle Memorial Institute
Columbus 1, Ohio

51 M. Cohen
Massachusetts Institute of Technology
Cambridge 39, Massachusetts

52 E. Wainer
Horizons Incorporated
Cleveland, Ohio

53 E. I. Larsen
P. R. Mallory & Company
Indianapolis, Indiana

54 O. C. Ralston
Metallurgy Division
Bureau of Mines
Department of Interior
Washington 25, D.C.

55 Supervisor
Metals Research
Armour Research Foundation
Chicago, Illinois

56 Dr. A. R. Troiano
Department of Metallurgical Engineering
Case Institute of Technology
University Circle
Cleveland 6, Ohio

57 Argonne National Laboratory
P. O. Box 299
Lemont, Illinois
Attn: Dr. Hoylande D. Young

58 - 59 U. S. Atomic Energy Commission
1901 Constitution Avenue, N.W.
Washington 25, D.C.
Attn: B. M. Fry

60 Brookhaven National Laboratory
Technical Information Division
Upton, Long Island, New York
Attn: Research Library

61 Carbide and Carbon Chemicals Division
Plant Records Department, Central Files (K-25)
P. O. Box P
Oak Ridge, Tennessee

62 Carbide and Carbon Chemicals Division
Central Reports and Information Office (Y-12)
P. O. Box P
Oak Ridge, Tennessee

63 General Electric Company
Technical Services Division
Technical Information Group
P. O. Box 100
Richland, Washington
Attn: Miss M. G. Freidank

64 Iowa State College
P. O. Box 14A, Station A
Ames, Iowa
Attn: Dr. F. H. Spedding

65 Knolls Atomic Power Laboratory
P. O. Box 1072
Schenectady, New York
Attn: Document Librarian

66 Los Alamos Scientific Laboratory
P. O. Box 1663
Los Alamos, New Mexico
Attn: Document Custodian

67 Mound Laboratory
U. S. Atomic Energy Commission
P. O. Box 32
Miamisburg, Ohio
Attn: Dr. M. M. Haring

68 U. S. Atomic Energy Commission
New York Operations Office
P. O. Box 30, Ansonia Station
New York 23, New York
Attn: Division of Technical Information
and Declassification Service

69 Oak Ridge National Laboratory
P. O. Box P
Oak Ridge, Tennessee
Attn: Central Files

70 Sandia Corporation
Sandia Base
Classified Document Division
Albuquerque, New Mexico
Attn: Mr. Dale N. Evans

71 U. S. Atomic Energy Commission
Library Branch, Technical Information
Service, ORE
P. O. Box E
Oak Ridge, Tennessee

72 University of California
Radiation Laboratory
Information Division
Room 128, Building 50
Berkeley, California
Attn: Dr. R. K. Wakerling

73 Westinghouse Electric Corporation
Atomic Power Division
P. O. Box 1468
Pittsburgh 30, Pennsylvania
Attn: Librarian

74 Commander
U. S. Naval Proving Ground
Dahlgren, Virginia

75 Metallurgy Group (WCRRL)
Flight Research Laboratory
Wright Air Development Center
Wright-Patterson Air Force Base
Dayton, Ohio

76 Dr. Max Hansen, Chairman
Metals Research Department
Armour Research Foundation
Technology Center
Chicago 16, Illinois

77 Office of Ordnance Research
Duke University
2127 Myrtle Drive
Durham, North Carolina
Attn: Dr. A. G. Guy

78 Office of Technical Service
Department of Commerce
Washington 25, D.C.

79 - 83 Armed Services Technical Information Agency
Documents Service Center
Knott Building
Dayton 2, Ohio

84 E. S. Machlin
Assistant Professor of Metallurgy
Columbia University
New York 27, New York